Mathematical Analysis and its Contemporary Applications
Volume 7, Issue 3, 2025, 77–113
doi: 10.30495/maca.2025.2063976.1141
ISSN 2716-9898

The novel hybrid approach for solving time-fractional Fokker-Planck equations by Tarig Projected Differential Transform method

Narsimhulu Dunna* and Athira Kinakkal

Abstract. Fractional models offer greater accuracy and efficiency in modelling various physical systems across scientific, engineering, and technological fields. Analyzing linear and nonlinear time-fractional systems of fractional order differential equations is a challenging task in terms of mathematical and theoretical aspects. In this paper, we propose a hybrid approach as a combination of the strength of the Tarig transform with the Projected Differential Transform Method (TPDTM) for solving the linear time-fractional Fokker-Planck (F-P) equation. The solution of the F-P equation was obtained in terms of space and fractional time co-ordinates based on imposing the different initial conditions. The results of the present work are illustrated using detailed $2D$ and $3D$ plots and tables for different values of the fractional parameter, providing visual and numerical clarity on the behavior of the solutions. To validate the solution and evaluate the algorithmic performance of the TPDTM, we have performed comparative analysis against solutions obtained using the Finite Difference Method (FDM), Homotopy Perturbation Method (HPM), and Laplace Adomian Decomposition Method (LADM) through different time fractional F-P equations. The study investigates solutions that show that TPDTM is a potent and straightforward technique for interpreting fractional F-P equations and is more versatile than FDM and HPM. Also, we found that our present work interpreted the high effectiveness and accuracy precision of results.

Keywords: Fractional differential calculus, Fokker-Planck equation, Tarig transform, Projected differential transform method, Numerical simulation

2020 Mathematics Subject Classification: 34K37, 26A33

*Corresponding author

1. Introduction

Fractional calculus is a crucial branch of mathematics, and it extends the concept of integrals and derivatives to arbitrary, non-integer order. The history of fractional models is extensive and well-established. Over the past decades, several notable figures in mathematics, physics, and applied mathematics have significantly contributed to the field. These include Cauchy, Liebniz, Liouville, Abel, Caputo, Riesz, and many more. Most mathematical theories pertinent to fractional calculus were developed before the 20^{th} century. Also, it has been noted that many real-world problems and examples of fractional calculus emerged in the 20^{th} century. By no means are these applications and the mathematical basis of fractional calculus illogical, but it is a challenging task to comprehend the physical meaning [47]. There has been a remarkable surge in the advancement of fractional differential equations driven by their broad scope and applications in various fields of science and technology, including control and signal analysis [2, 30, 82], biology [70], mechanical engineering [47], chemical engineering [79], for instance, as colored noise [56], boundary layer effects in dust [1, 37], heat transfer [54], electromagnetic waves [38], electrode-electrolyte polarization [41], image processing [16], synchronization of chaos [22], viscoelasticity [49, 55], multidirectional multi scroll attractors [24], and friction modeling [59], etc. The majority of physical, mechanical, engineering, and biological problems in the modern era are represented as nonlinear fractional partial differential equations and have been subjected to many efficient methods, including the fractional variation iteration method (VIM) [19], Inverse scattering transform (IS) [36, 32], fractional differential transform method (DTM) [28], fractional operational matrix method (OMM) [45], fractional improved homotopy perturbation method (IHPM) [46], fractional wavelet method (WM) [71], and fractional Laplace Adomian decomposition method (LADM) [61].

Considerable research has been conducted to derive exact and approximate solutions for a wide range of partial and fractional differential equations (linear and nonlinear). For instance, Schrödinger equation [36], Hirota equations [31], the Kadomtsev–Petviashvili equation [35], the KdV–Calogero–Bogoyavlenskii–Schiff equation [33] the Sharma–Tasso–Olver [34], the time-fractional Zakharov- Kuznetsov (ZKE) [78], Burgers-Huxley (BH) [64], Noyes-Field (NF) model of Belousov-Zhabotinsky (BZ) [5], Benjamin Bona Mahony Burger (BBMB) [63], Poisson (P) [68], Telegraph (TE), Laplace (L), wave (W) equations [18], and Newell-Whitehead-Segel equations (N-W-S)[4]. In this research, we are finding the solutions of Fokker-Planck (F-P) equation . The understanding of solution of F-P equation is crucial, due to its potential applications in various fields of natural science by modeling the time evolution for systems influenced by stochastic (random) processes, such as solid-state physics, quantum optics, chemical physics, theoretical biology, circuit theory, plasma physics,

surface physics, population dynamics, biophysics, engineering, neuroscience, nonlinear hydrodynamics, polymer physics, laser physics, pattern formation, psychology, and marketing.

The nonlinear F-P equation in a single variable scenario expressed as follows:

$$\frac{\partial U}{\partial t} = \left(-\frac{\partial}{\partial x} A(x,t,U) + \frac{\partial^2}{\partial x^2} B(x,t,U) \right) U(x,t). \tag{1}$$

In this work, we focus on the time fractional F-P equation of the form

$$\frac{\partial^\alpha U}{\partial t} = \left(-\frac{\partial}{\partial x} A(x,t,U) + \frac{\partial^2}{\partial x^2} B(x,t,U) \right) U(x,t),\ t > 0, \text{ and } \alpha \in (0,1], \tag{2}$$

where α is the order of fractional time, A and $B > 0$ are the drift coefficient and the diffusion coefficient respectively. Time may also affect the drift and diffusion coefficients. If $\alpha = 1$, the time fractional F-P equation (2) reduced to a nonlinear classical F-P equation.

From the early century onwards, researchers have been interested in finding the solution to the F-P equation. In 1996, Drozdov and Morillo [25] proposed a finite-difference method (FDM) to solve a general class of linear and non-linear time-dependent F-P equations based on a K- point Stirling interpolation algorithm. To solve several linear and nonlinear space-time F-P equations in closed form, Dubay et al. [26] suggested an effective method based on the Homotopy perturbation method (HPM) employing the Sumudu transform (ST). Johnson et al. [29] used the convergence of a class of combined spectral-finite difference methods (S-FDM) using the Hermine basis to study the F-P equation. Tatari et al. [69] investigated the solution of the F-P equation and some similar equations through the Adomian Decomposition method (ADM). Dehghan and Tatari [21] used VIM as proposed by Chinese mathematician Ji Huan He to solve the F-P equation. Pankaj and Narayanan [51] used the standard sequential finite element method (FEM) with shape functions and the Crank-Nicholson time integration scheme (C-N TIS) to examine the numerical solution of both the stationary and transient variants of the F-P equation for two-state nonlinear systems. Biazar [10] employed HPM in 2008 to solve the linear and nonlinear F-P equation. HPM has been generalized by Jafari and Aminataei [42]. They demonstrated that the HPM, the spectral method (SM), and ADM are all special cases of newly modified HPM; they used the generalized version of HPM to solve the F-P equation in their research. Yang et al. [74] examined a family of time and space fractional F-P equation, using the Riesz space fractional derivative of order $\mu \in (1,2)$ and the Riemann Lioville time fractional derivative of order $1-\alpha$. Yildirim [75] investigated the numerical solution of the F-P equation and some similar equations using the HPM. The primary goal of his study was to suggest a different approach to solve the problem that isn't dependent on spectral, finite difference, or finite element methods. The space

and time fractional F-P equation can be numerically solved using FEM created by Weihua [23]. This method is useful for characterizing processes that involve both flight and trapping. Zhengang and Changpin [77] solved the extended non-linear F-P equation using a completely discrete Galerkin FEM. A dynamic interval Shannon wavelet collocation approach for fractional F-P equations was proposed by Shu and De [57] in 2013. Ayati et al. [6] solved the space-time dependent fractional F-P equation using a new form of the HPM in 2014. In 2015, Mohamed et al. [58] offered an approximate analytical solution using the fractional iteration method (IM) for the time fractional F-P equation. In 2016, Jawary [3] solved the linear and nonlinear F-P equation as well as a few other equations of a similar nature using the new iterative method (NIM) developed by Daftardar-Gejji and Jafari in 2006. Hemeda and Eladdad [39] introduced a new integral iterative method (NIIM) in 2018 to solve linear and nonlinear F-P and similar equations. Apart from this, several research works [9, 11, 12, 13, 14, 20, 43, 48, 50, 52, 62, 67, 72, 80, 81] have been conducted on the F-P equation because of its tremendous applications.

Recently, Behnam and Marzieh [66] used a compact finite difference method to find the numerical solution of the F-P equation. Yoong et al. [73] presented a brand-new machine learning technique based on deep neural networks in 2019 to solve the general F-P equations. A new conformable Laplace decomposition method (LDM) was developed by Muammer and Ozan [7] to solve the nonlinear fractional F-P problem.

Even though semi-analytical techniques like HPM and LADM are widely used to solve nonlinear differential equations, they frequently have drawbacks when used to solve problems involving complex terms, singular perturbations, or strong nonlinearity. In particular, HPM necessitates a suitable selection of embedding parameters and may not exhibit consistent convergence throughout the domain, whereas LADM may experience slow convergence and accumulation of Adomian polynomials. The Tarig Projected Differential Transform Method (TPDTM) [8], as a blending of the Tarig Transform [27] with the Projected Differential Transform Method (PDTM) [44], on the other hand provides a more effective substitute by projecting the solution space to lower dimensional complexity, which enhances computing performance and lowers memory needs. Additionally, TPDTM has a wider stability region, which makes it better suited for problems where traditional approaches become computationally demanding or unstable.

In this paper, we use this novel TPDTM for solving the linear time-fractional F-P. Nevertheless, no researcher has yet examined the solution to the well-known F-P equation using the suggested hybrid technique (TPDTM). Athira et al. [4] proposed TPDTM in their research work for finding the solutions of N-W-S and Burgers equation and they concluded with the efficiency and reliability, stability of the method on other powerful methods existing in literature. From the literature,

it is evident that, this is the first time, we employed the TPDTM approach to compute numerical approximate solutions for the F-P equation, motivated by the work of Athira et al. in the existing literature.

The organization of the paper is outlined below: Section 2 discusses specific vocabulary and the mathematical underpinnings of the fractional calculus theory to establish our results. To test the effectiveness of our method, we solve the fractional-order F-P equation in Section 3. The numerical outcomes and their analysis are presented in Section 4, followed by the study's conclusions and summary in Section 5.

2. Methodology

2.1. Basic Definitions. This section introduces some basic definitions:

Definition 2.1. [65] The Reimann-Liouville fractional integral of order α of a) left-sided for a function $f(t) \in L_1(a,b)$, $\alpha > 0$ as:

$$\left(I^{\alpha}_{a^+} f\right)(t) = \frac{1}{\Gamma(\alpha)} \int_a^{\infty} (t-s)^{\alpha-1} f(s)\, ds, \quad s > \alpha.$$

b) right-sided for a function $f(t) \in L_1(a,b)$, $\alpha > 0$ as:

$$\left(I^{\alpha}_{b^-} f\right)(t) = \frac{1}{\Gamma(\alpha)} \int_{-\infty}^{b} (t-s)^{\alpha-1} f(s)\, ds, \quad s < \alpha.$$

Definition 2.2. [65] The Riemann integral on the half axis subjected to variable limit can be defined as

$$\left(I^{\alpha}_{0^+} f\right)(t) = \frac{1}{\Gamma(\alpha)} \int_a^{\infty} (t-s)^{\alpha-1} f(s)\, ds, \quad 0 < t < \infty.$$

Definition 2.3. [65] The Reimann-Liouville fractional derivative of order α, $0 < \alpha < 1$ in the interval $[a,b]$ of

a) left-sided for a function $f(t)$ defined as

$$\left(D^{\alpha}_{a^+} f\right)(t) = \frac{1}{\Gamma(1-\alpha)} \frac{d}{dt} \int_a^{t} (t-s)^{-\alpha} f(s)\, ds.$$

b) right-sided for a function $f(t)$ defined as

$$\left(D^{\alpha}_{b^-} f\right)(t) = \frac{1}{\Gamma(1-\alpha)} \frac{d}{dt} \int_t^{b} (t-s)^{-\alpha} f(s)\, ds.$$

Definition 2.4. [15] The fractional derivative of $f(t)$ in the Caputo, sense is defined for $n-1 < \alpha \leq n$, $n \in N$, $t > 0$ by

$$D^{\alpha} f(t) = \frac{1}{\Gamma(n-\alpha)} \int_0^{t} (t-s)^{n-\alpha-1} f^{(n)}(s)\, ds.$$

Definition 2.5. [53] The generalization of the exponential function, the Mittag-Leffler function, is defined for $\alpha \in C$, $Re(\alpha) > 0$, by

$$E_\alpha(Z) = \sum_{n=0}^{\infty} \frac{Z^n}{\Gamma(n\alpha + 1)}.$$

2.2. Tarig Transform. The Tarig transforms of a time domain function, $f(t)$ [27] is defined as follows:

$$T[f(t)] = \frac{1}{\vartheta} \int_0^\infty e^{-\frac{t}{\vartheta^2}} f(t)\, dt, \quad \vartheta \neq 0, \tag{3}$$

where ϑ is the frequency domain variable. Let $f(t)$ is a temporal function, then its corresponding frequency space function representation through the Tarig Transform is denoted by $F(\vartheta)$. If $F(\vartheta)$ is the Tarig transform of $f(t)$ of order α, the Tarig transform of the fractional integral of $f(t)$ with order α [27] is:

$$T\left[(I_{0+}^{\alpha} f)(t)\right] = \vartheta^{2\alpha} F(\vartheta) = \vartheta^{2\alpha} T[f(t)]. \tag{4}$$

In a similar way, the Tarig transform of the fractional derivative of $f(t)$ with order α [8] is;

$$T\left[D^{\alpha} f(t)\right] = F^{\alpha}(\vartheta) = \frac{1}{\vartheta^{2\alpha}} F(\vartheta) - \sum_{i=1}^{n} \vartheta^{2(i-\alpha)-1} f^{(i-1)}(0). \tag{5}$$

2.3. Projected Differential Transform Method (PDTM) Definition, Property and Theorem. If $f(s_1, s_2, \ldots, s_n)$ is a multivariable function, its PDTM can be defined [44] as follows:

$$f(s_1, s_2, \ldots, s_{n-1}, k) = \frac{1}{k!} \left[\frac{\partial^k f(s_1, s_2, \ldots, s_n)}{\partial s_n^k} \right]_{s_n}, \tag{6}$$

where f denotes the n-dimensional base function in terms of $s_1, s_2, \ldots, s_n$. The differential inverse transform of $f(s_1, s_2, \ldots, s_{n-1}, k)$ can be defined [44] as follows:

$$f(s_1, s_2, \ldots, s_n) = \sum_{k=0}^{\infty} f(s_1, s_2, \ldots, s_{n-1}, k)\, (s - s_0)^k. \tag{7}$$

Now, we present some fundamental theorems obtained by the PDTM that are relevant to our work. Let $u(s_1, s_2, \ldots, s_n)$ and $v(s_1, s_2, \ldots, s_n)$ be any two multi variable functions and $u(s_1, s_2, \ldots, s_{n-1}, k)$ and $v(s_1, s_2, \ldots, s_{n-1}, k)$ are the respective transforms of the u and v respectively. Fix c be an arbitrary constant.

- Given $z(s_1, s_2, \ldots, s_n) = u(s_1, s_2, \ldots, s_n) v(s_1, s_2, \ldots, s_n)$, it follows that

$$z(s_1, s_2, \ldots, s_{n-1}, k) = u(s_1, s_2, \ldots, s_{n-1}, k) v(s_1, s_2, \ldots, s_{n-1}, k).$$

- Given $z(s_1, s_2, \ldots, s_n) = cu(s_1, s_2, \ldots, s_n)$, it follows that

$$z(s_1, s_2, \ldots, s_{n-1}, k) = cu(s_1, s_2, \ldots, s_{n-1}, k).$$

- Given $z(s_1, s_2, \ldots, s_n) = \frac{d^n u(s_1, s_2, \ldots, s_n)}{(ds_n^n)}$, it follows that

$$z(s_1, s_2, \ldots, s_{n-1}, k) = \frac{(k+n)}{k!} u(s_1, s_2, \ldots, s_{n-1}, k+n).$$

- Given $z(s_1, s_2, \ldots, s_n) = u(s_1, s_2, \ldots, s_n)v(s_1, s_2, \ldots, s_n)$, it follows that

$$z(s_1, s_2, \ldots, s_{n-1}, k) = \sum_{m=0}^{k} u(s_1, s_2, \ldots, s_{n-1}, m)v(s_1, s_2, \ldots, s_{n-1}, m).$$

- Given $z(s_1, s_2, \ldots, s_n) = u_1(s_1, s_2, \ldots, s_n)u_2(s_1, s_2, \ldots, s_n)...u_n(s_1, s_2, \ldots, s_n)$, it follows that

$$z(s_1, s_2, \ldots, s_{n-1}, k) = \sum_{k_{n-1}=0}^{k} \sum_{k_{n-2}=0}^{k_{n-1}} \cdots \sum_{k_2=0}^{k_3} \sum_{k_1=0}^{k_2} u_1(s_1, s_2, \ldots, s_{n-1}, k_1)$$
$$u_2(s_1, s_2, \ldots, s_{n-1}, k_2 - k_1)...u_{n-1}(s_1, s_2, \ldots, s_{n-1},$$
$$k_{n-1} - k_{n-2})u_n(s_1, s_2, \ldots, s_{n-1}, k - k_{n-1}).$$

2.4. TPDTM Methodology. Consider the nonlinear time-fractional differential equation

$$[D^\alpha + R + N]U(x,t) = g(x,t), \tag{8}$$

subjected to the rudimentary:

$$U(x,0) = f(x), \tag{9}$$

In this context, $D^\alpha = \frac{\partial^\alpha}{\partial t^\alpha}$ is the fractional order derivative operator, where R and N correspond to the linear and nonlinear differential operators, respectively, and $g(x,t)$ represents the source term.
By applying the Tarig transform (T) on both sides of equation (8), we get [8]

$$T[D^\alpha U(x,t)] + T[RU(x,t)] + T[NU(x,t)] = T[g(x,t)]. \tag{10}$$

Using the differential property of Tarig transform equation (5) on equation(8) and equation(9), we get [8]

$$T[D^\alpha U(x,t)] = \vartheta f(x) + \vartheta^{2\alpha}[T[g(x,t)] - T[RU(x,t)] + T[NU(x,t)]] \tag{11}$$

Taking the inverse Tarig transform to the Eqn. (11), then we have [8]

$$U(x,t) = G(x,t) - T^{-1}[\vartheta^{2\alpha}[T[RU(x,t)] + T[NU(x,t)]]], \tag{12}$$

where $G(x,t)$ represent the term arise from the source term and the initial condition. Using PDTM, the non-linear term can be decomposed as [8]:

$$U(x, m+1) = -T^{-1}[\vartheta^{2\alpha} T[RU(x,t)] + T[NU(x,t)]], m \geq 0, U(x,0) = f(x). \tag{13}$$

The closed-form solution for equations (8)-(9) takes the form of a series:

$$U(x,t) = \sum_{m=0}^{\infty} U(x,m) \tag{14}$$

with all component, $U(x,m)$ being derived based on the spatial variable (x) and time (t)

2.5. Errors, Convergence and Stability Criteria. A thorough convergence analysis is necessary to establish the trustworthiness of the TPDTM-derived series solution in Eq.(14). The approximate solution of the equation (8) with initial condition equation (9) can be obtained [8] as:

$$U_{app(n)}(x,t) = \sum_{m=0}^{n} U(x,m).$$

By discarding higher-order terms $(m > n)$ in the summation in equation (14) the exact solution of equation (8) and equation (9) is represented [8] as:

$$U(x,t) = U_{app(n)}(x,t) + e_n U(x,t), \tag{15}$$

where $e_n U(x,t)$ is the error function. In general, the absolute error is defined by

$$e_n U(x,t) = |\sum_{m=0}^{\infty} U(x,m) - U_{app(n)}(x,t)|.$$

For the highly practical scenarios, a closed-form solution, $U(x,t)$, is not possible. So, define the approximate absolute error [8] as:

$$E_n U(x,t) = |U_{app(n)}(x,t) - U_{app(n+1)}(x,t)|.$$

Demonstrating convergence for equation (14) requires proving that $E_n U(x,t)$ forms an approaching sequence. As this sequence $E_n U(x,t)$ has a lower bound, establishing its monotonic decreasing nature would suffice to guarantee convergence. Hence, the convergence criteria [8] is $\left|\frac{E_h U(x,t)}{E_n U(x,t)}\right| < 1$, for $n < h$. Using the following algorithm, the convergence of the iterative solution $U_{app(n)}(x,t)$ to exact solution $U(x,t)$ can be shown as following 4 steps [8].

(1) Determine $U_{app(n)}(x,t)$, $U_{app(n+1)}(x,t)$.
(2) Determine $U_{app(h)}(x,t)$, $U_{app(h+1)}(x,t), n \leq h$
(3) Delineate
$E_n U(x,t) = |(U_{app(n)} - U_{app(n+1)})(x,t)|$,
$E_h U(x,t) = |(U_{app(h)} - U_{app(h+1)})(x,t)|$, for some x and t.
(4) If $E_n U(x,t) \geq E_h U(x,t)$, then $U_{app(n)}(x,t)$ achieves the true solution $U(x,t)$, as $n \to \infty$.

The proposed method is utilized to rigorously establish the convergence of the series solution obtained through TPDTM. If the series converges, then it is stable.

Theorem 2.1 (Contractivity of the TPDTM Iteration)**.** *Let $(X, \|\cdot\|)$ be a Banach space of functions associated with the TPDTM iterates happen Define the linear operator*

$$\mathcal{O} := T^{-1}\left[\vartheta^{2\alpha} T(\cdot)\right],$$

and consider the TPDTM iteration written in operator form

$$U_{m+1} = \Phi(U_m), \qquad \Phi(U) := -\mathcal{O}\big(RU + NU\big), \tag{16}$$

where $R : X \to X$ is linear and bounded and $N : X \to X$ is nonlinear. Assume:

(1) *$\mathcal{O} : X \to X$ is linear and bounded with $\|\mathcal{O}\| = b$.*
(2) *$R : X \to X$ is linear and bounded with operator norm $\|R\|$.*
(3) *$N : X \to X$ is Lipschitz on the relevant solution ball in X with Lipschitz constant K, i.e.*

$$\|N(U - V)\| \le K\|U - V\|, \qquad \forall\ U, V \text{ in the ball.}$$

(4) *The constant*

$$q := b\big(\|R\| + L\big)$$

satisfies $0 \le q < 1$.

Then Φ is a contraction on the chosen ball in X, the sequence $\{U_m\}$ defined by equation (16) is contractive in the sense

$$\|U_{m+1} - U_m\| \le q\,\|U_m - U_{m-1}\|, \qquad m \ge 1,$$

and hence

$$\|U_{m+1} - U_m\| \le q^m \|U_1 - U_0\|.$$

Consequently $\{U_m\}$ converges (geometrically) to the unique fixed point $U \in X$ of Φ, and the tail estimate

$$\|U - U_m\| \le \frac{q^m}{1 - q}\,\|U_1 - U_0\|$$

holds for all $m \ge 0$.

Proof. To establish the contraction mapping Φ, consider arbitrary U, V in the solution ball of X and apply fundamental properties of TPDTM and its inverse, we can get

$$\begin{aligned}
\|\Phi(U) - \Phi(V)\| &= \big\| - \mathcal{O}\big(RU + NU\big) + \mathcal{O}\big(RV + NV\big)\big\| \\
&= \big\|\mathcal{O}\big(R(V - U) + N(V - U)\big)\big\| \\
&\le \|\mathcal{O}\|\ \big(\|R\|\,\|U - V\| + \|N(U - V)\|\big) \\
&\le b\big(\|R\| + K\big)\|U - V\| = q\|U - V\|.
\end{aligned}$$

Thus Φ is a contraction with constant $q \in [0, 1)$. Applying this bound to successive iterates U_m and U_{m-1}, we get

$$\|U_{m+1} - U_m\| = \|\Phi(U_m) - \Phi(U_{m-1})\| \le q\,\|U_m - U_{m-1}\|,$$

which is exactly the contractive inequality for the error differences. Continuing the iteration yields

$$\|U_{m+1} - U_m\| \le q^m \|U_1 - U_0\|.$$

Since, $0 \leq q < 1$, the geometric decay implies $\{U_m\}$ is Cauchy sequence: for $n > m$,

$$\|U_n - U_m\| \leq \sum_{j=m}^{n-1} \|U_{j+1} - U_j\| \leq \sum_{j=m}^{n-1} q^j \|U_1 - U_0\| = \frac{q^m(1-q^{n-m})}{1-q}\|U_1 - U_0\|.$$

Letting $n \to \infty$ shows $\{U_m\}$ converges to some $U \in X$. Passing to the limit in $U_{m+1} = \Phi(U_m)$ and using continuity of Φ (since Φ is contractive sequence) we get $\Phi(U) = U$, implies U is a fixed point.
Uniqueness of fixed point follows immediately: if V is another fixed point then

$$\|U - V\| = \|\Phi(U) - \Phi(V)\| \leq q\|U - V\|,$$

hence $\|U - V\| = 0$ and $U = V$. Finally, summing the geometric tail gives the error bound

$$\|U - U_m\| \leq \sum_{j=m}^{\infty} \|U_{j+1} - U_j\| \leq \sum_{j=m}^{\infty} q^j \|U_1 - U_0\| = \frac{q^m}{1-q}\|U_1 - U_0\|.$$

This completes the proof. □

Remark. If you prefer a pointwise statement; replace $\|\cdot\|$ by the pointwise absolute value $|\cdot|$ then the same derivation gives

$$|U(x, m+1) - U(x, m)| \leq q\,|U(x, m) - U(x, m-1)|$$

and thus the approximate error measure used in the manuscript,

$$E_m U(x,t) = \left|U_{\mathrm{app}(m+1)} - U_{\mathrm{app}(m)}\right| = |U(x, m+1)|,$$

satisfies $E_{m+1}U(x,t) \leq q\,E_m U(x,t)$. If the bound $q < 1$ cannot be shown globally, state it locally in time (choose t small enough) or on a solution ball where the Lipschitz constant K and the operator norm a are controlled.

Corollary 2.2 (Error-sequence contractivity)**.** *Under the hypotheses of Theorem 1, define the approximate error sequence (in norm)*

$$E_m U := \|U_{\mathrm{app}(m+1)} - U_{\mathrm{app}(m)}\| = \|U(m+1)\|$$

Then the error sequence is contractive:

$$\|U_{\mathrm{app}(m+2)} - U_{\mathrm{app}(m+1)}\| \leq q\,\|U_{\mathrm{app}(m+1)} - U_{\mathrm{app}(m)}\| \quad \textit{for all } m \geq 0,$$

hence

$$\|U_{\mathrm{app}(m+1)} - U_{\mathrm{app}(m)}\| \leq q^m \|U_{\mathrm{app}(1)} - U_{\mathrm{app}(0)}\|,$$

implies

$$\|U - U_{\mathrm{app}}(m)\| \leq \frac{q^m}{1-q}\,\|U_{\mathrm{app}(1)} - U_{\mathrm{app}(0)}\|,$$

and for any indices $h > n$,

$$\frac{E_h U}{E_n U} \leq q^{h-n} < 1.$$

PROOF. Subtract two successive recurrences:

$$\begin{aligned} U(m+1)-U(m) &= -\mathcal{O}\big(RU(m)+NU(m)\big)+\mathcal{O}\big(RU(m-1)+NU(m-1)\big) \\ &= -\mathcal{O}\Big(RU(m)-RU(m-1)\big)+\big(NU(m)-NU(m-1)\Big). \end{aligned}$$

Taking norms and using linearity,boundedness of $\mathcal{O}$ and R, and the Lipschitz property of N, we obtain

$$\begin{aligned} E_{m+1}U &= \|U(m+1)-U(m)\| \\ &\le \|\mathcal{O}\|\Big(\|R\|\,\|U(m)-U(m-1)\|+\|NU(m)-NU(m-1)\|\Big) \\ &\le b\big(\|R\|+K\big)\,\|U(m)-U(m-1)\| \\ &= q\,E_mU. \end{aligned}$$

Iterating gives $E_mU \le q^m E_0U$ and the geometric tail bound follows by summation:

$$\|U-U_{\mathrm{app}(m)}\| \le \sum_{j=m}^{\infty} EU_j \le \sum_{j=m}^{\infty} q^j EU_0 = \frac{q^m}{1-q}EU_0.$$

Finally for any $h > n$,

$$\frac{E_hU}{E_nU} \le \frac{q^h EU_0}{q^n EU_0} = q^{h-n} < 1,$$

This completes the proof. □

3. Numerical Test Examples

Test Example 1. The F-P equation,

$$D^\alpha U-(U_{xx}+U_x)=0, \alpha\in(0,1],$$

is derived from the F-P equation (2) by putting $A=-1$ and $B=1$. Our work focuses on the linear time-fractional Fokker-Planck equation given by:

$$D^\alpha U = U_{xx}+U_x, \alpha\in(0,1], \tag{17}$$

subject to the initial condition $U(x)=x$ at $t=0$. By taking the Tarig transform of equation (17), together with the initial condition, we obtain:

$$T[U(x,t)] = \vartheta x - \vartheta^{2\alpha}[T[U_{xx}+U_x]] \tag{18}$$

Applying inverse Tarig transform on both sides of equation (18), since $T^{-1}(\vartheta)=1$, we get

$$U(x,t)+T^{-1}[\vartheta^{2\alpha}[T[U_{xx}+U_x]]]-x=0, \tag{19}$$

equation (19) is transformed using the PDTM, yielding

$$U(x,m+1)+T^{-1}\vartheta^{2\alpha}[T[U_{xx}+U_x]]]=0, \tag{20}$$

FDM Implementation Steps [17]
Step 1: Begin with the given PDE and define both temporal and spatial domains. Discretize these domains using appropriate grid spacing. Step 2: Replace all derivatives in the PDE with their finite difference approximations, converting the differential equation into a system of algebraic equations. Step 3: Incorporate boundary conditions into the discretized system, then solve the resulting equations using an iterative computational approach. Step 4: Save the final numerical solution in the form $U(x,t)$ for further analysis and visualization.
LADM Implementation [76]
Step 1: Start with the given PDE and its initial conditions. Apply the Laplace transform to convert the PDE into an algebraic form in the Laplace domain. Step 2: Express any nonlinear terms in the equation using Adomian polynomials, which systematically break down nonlinearities into a computable series. Step 3: Solve the transformed equation iteratively, constructing successive approximations until the desired level of accuracy is achieved. Step 4: Finally, apply the inverse Laplace transform to revert the solution back to the original domain, yielding the approximate solution $U(x,t)$.
HPM Implementation [75]
Step 1: Start with the given PDE and its initial conditions and construct the homotopy by introducing an embedding parameter p. Step 2: Expand the solution as a power series in p, substitute into the homotopy equation, and collect like powers of p. Step 3: The resulting system is solved through successive iteration. Step 4: Obtain the approximate solution $U(x,t)$ by setting $p=1$.

Based on the equation (20), we obtain:

$$U(x,1)=\frac{t^{\alpha}}{\Gamma(\alpha+1)}, U(x,2)=U(x,3)=U(x,4)=...,U(x,n)=0.$$

Following the same recursive procedure, we generate the complete sequence of approximation. The resulting series solution of system of equation (17) via TPDTM takes the form:

$$U(x,t)-x=\frac{t^{\alpha}}{\Gamma(\alpha+1)}.$$

Test Example 2. The F-P equation,

$$D^{\alpha}U=xU_{xx}-xU_{x}, \alpha\in(0,1],$$

is derived from the F-P equation (2) by putting $A=x$ and $B=x$. Our work focuses on the linear time-fractional Fokker-Planck equation given by:

$$D^{\alpha}U=xU_{xx}-xU_{x}, \alpha\in(0,1], \tag{21}$$

under the initial circumstances $U(x) = x$ at $t = 0$. Apply the Tarig transform to the left and right sides of the equation (21), then obtain:

$$T[U(x,t)] = [\vartheta x + \vartheta^{2\alpha}[T[xU_{xx} - xU_x]] \tag{22}$$

Taking the inverse Tarig transform to the equation (22), and since $T^{-1}(\vartheta) = 1$, then obtain

$$U(x,t) = x + T^{-1}[\vartheta^{2\alpha}[T[xU_{xx} - xU_x]]], \tag{23}$$

Using PDTM, equation (23) becomes

$$U(x, m+1) = T^{-1}\vartheta^{2\alpha}[T[xU_{xx} - xU_x]]. \tag{24}$$

Based on the equation (24), the following expression is obtained:

$$U(x,1) = -x\frac{t^{\alpha}}{\Gamma(\alpha+1)}, U(x,2) = x\frac{t^{2\alpha}}{\Gamma(2\alpha+1)}, U(x,3) = -x\frac{t^{3\alpha}}{\Gamma(3\alpha+1)},$$

$$U(x,4) = x\frac{t^{4\alpha}}{\Gamma(4\alpha+1)}, ..., U(x,n) = (-1)^n x\frac{t^{n\alpha}}{\Gamma(n\alpha+1)}.$$

Following the same recursive procedure, we generate the complete sequence of approximation. The resulting series solution of system of equation (20) via TPDTM takes the form:

$$U(x,t) = x + \sum_{k=1}^{\infty}(-1)^k \frac{xt^{\alpha}}{\Gamma(k\alpha+1)}.$$

Test Example 3. The F-P equation,

$$D^{\alpha}U = xU_{xx} - xU_x, \alpha \in (0,1],$$

is derived from the F-P equation (2) by putting $A = x$ and $B = x$.

Our work focuses on the linear time-fractional Fokker-Planck equation given by:

$$D^{\alpha}U = xU_{xx} - xU_x, \alpha \in (0,1], \tag{25}$$

with the initial condition $U(x) = x^2$ at $t = 0$. The Tarig transform is applied to equation (25), and the required result is:

$$T[U(x,t)] = \vartheta x^2 + \vartheta^{2\alpha}[T[xU_{xx} - xU_x]]. \tag{26}$$

Inverting the Tarig transform to the equation (26) and using $T^{-1}(\vartheta) = 1$, we get

$$U(x,t) = x^2 + T^{-1}[\vartheta^{2\alpha}[T[xU_{xx} - xU_x]]], \tag{27}$$

Using PDTM, equation (27) becomes to

$$U(x, m+1) - T^{-1}[\ \vartheta^{2\alpha}[T[xU_{xx} - xU_x]]]. = 0 \tag{28}$$

Based on the equation (28), yielding:

$$U(x,1) = (2x - 2x^2)\frac{t^{\alpha}}{\Gamma(\alpha+1)}, U(x,2) = (4x^2 - 6x)\frac{t^{2\alpha}}{\Gamma(2\alpha+1)},$$

$$U(x,3) = (14x - 8x^2)\frac{t^{3\alpha}}{\Gamma(3\alpha+1)}, ...,$$

$$U(x,n) = ((2n^2 - 2n + 2)x + (-1)^n 2^n x^2)\frac{t^{n\alpha}}{\Gamma(n\alpha+1)}.$$

Following the same recursive procedure, we generate the complete sequence of approximation. The resulting series solution of system of equation (25) via TPDTM takes the form:

$$U(x,t) = x^2 + \sum_{k=1}^{\infty}(-1)^{k+1}((2k^2 - 2k + 2)x + (-1)^k 2^k x^2)\frac{t^{k\alpha}}{\Gamma(k\alpha+1)}.$$

Test Example 4. The F-P equation,

$$D^\alpha U = U_{xx} + U_x, \alpha \in (0,1]$$

is obtained from the F-P equation (2) by putting $A = -1$ and $B = 1$. Our work focuses on the linear time-fractional Fokker-Planck equation given by:

$$D^\alpha U = U_{xx} + U_x, \alpha \in (0,1] \tag{29}$$

with initial condition $U(x) = x^2$ at $t = 0$. Apply the Tarig transform on both sides of the equation (29), we get:

$$T[U(x,t)] - \vartheta x^2 + \vartheta^{2\alpha}[T[U_{xx} + U_x]] = 0 \tag{30}$$

using the inverse property of Tarig transform on sides of equation (30), and since $T^{-1}(\vartheta) = 1$, we get :

$$U(x,t) - x^2 + T^{-1}\vartheta^{2\alpha}[T[U_{xx} + U_x]] = 0, \tag{31}$$

Equation (31) transformed using the PDTM,

$$U(x,m+1) + T^{-1}\vartheta^{2\alpha}[T[U_{xx} + U_x]] = 0, \tag{32}$$

Then then equation (32), implies:

$$U(x,1) = (2x+2)\frac{t^\alpha}{\Gamma(\alpha+1)}, U(x,2) = 2\frac{t^{2\alpha}}{\Gamma(2\alpha+1)}, U(x,3) = 0,$$

$$U(x,4) = 0, ..., U(x,n) = 0.$$

Following the same recursive procedure, we generate the complete sequence of approximation. The resulting series solution of system of equation (29) via TPDTM takes the form:

$$U(x,t) = x^2 + (2x+2)\frac{t^\alpha}{\Gamma(\alpha+1)} + 2\frac{t^{2\alpha}}{\Gamma(2\alpha+1)}.$$

3.1. Von–Neumann stability for Examples 1 and 4 (constant-coefficient spatial operator). Consider the linear TPDTM recurrence in the purely linear case ($N \equiv 0$)

$$U_{m+1} \;=\; -\mathcal{O}\big(RU_m\big),$$

where

$$\mathcal{O} := T^{-1}[\vartheta^{2\alpha} T(\cdot)]$$

is linear operator and acts as a bounded Fourier multiplier with operator norm $b = \|\mathcal{O}\|$. We analyse mode wise stability under periodic boundary conditions.
In test example 1 and 4: $R = \partial_{xx} + \partial_x$.

For a Fourier mode $e^{\mathrm{i}kx}$ we have the symbol

$$r(k) = -k^2 + \mathrm{i}k.$$

Hence the TPDTM recurrence reduces, modewise, to

$$\widehat{U}_{m+1}(k) = g(k)\,\widehat{U}_m(k), \qquad g(k) = -\widehat{\mathcal{O}}(k)\,r(k).$$

Using the bound $|\widehat{\mathcal{O}}(k)| \le b$ we obtain the conservative estimate

$$|g(k)| \le b\,|r(k)| = b\sqrt{k^4 + k^2} = b\,|k|\sqrt{k^2+1}.$$

Von–Neumann stability condition (practical form) [40, 60]**.** For every representable wave number k on the computational grid (or for all k in the Fourier continuum when the operator multiplier is sufficiently decaying) require

$$|g(k)| \le 1 \quad\Longleftrightarrow\quad b\,|k|\sqrt{k^2+1} \le 1.$$

On an unbounded continuous domain, $\sup_k |k|\sqrt{k^2+1} = \infty$, so the condition cannot hold globally; in practice the domain is either periodic/discrete (so k is bounded by $k_{\max}$) or one ensures b is sufficiently small (for example by restricting the time-window or choosing transform parameters) so that

$$b\,k_{\max}\sqrt{k_{\max}^2+1} < 1.$$

Connection to contractivity [40, 60]**.** If we denote the operator norm $\|R\|_{\mathrm{op}} := \sup_{|k|\le k_{\max}} |r(k)|$, the von–Neumann condition is implied by

$$b\,\|R\|_{\mathrm{op}} < 1,$$

which is exactly the linear part of the contractivity condition $q = b(\|R\| + K) < 1$ (with $K = 0$ here). Under this inequality every Fourier mode decays (i.e. $|g(k)| < 1$), hence the iteration is stable and successive differences decay geometrically.

3.2. Energy (weighted) stability for Examples 2 and 3 (variable coefficients). Consider the linear equation in test example 2 and 3:

$$D^\alpha U = xU_{xx} - xU_x$$

on a spatial interval $\Omega = [x_0, x_1]$ with $0 < x_0 < x_1 < \infty$. Assume homogeneous boundary conditions (Dirichlet or boundary terms that make the integrations by parts vanish) and sufficiently smooth U. Define the weighted inner product and norm

$$(U, V)_w := \int_{x_0}^{x_1} w(x)\, U(x) V(x)\, dx, \qquad \|u\|_w^2 = (U, V)_w,$$

with weight $w(x) = x$ (positive on Ω).

Multiply the PDE by $w(x)U(x,t)$ and integrate over Ω:

$$\left(wU, D^\alpha U\right) = \int_{x_0}^{x_1} xU\, D^\alpha U\, dx = \int_{x_0}^{x_1} xU\, (xU_{xx} - xU_x)\, dx.$$

Focus on the right-hand side and integrate by parts (boundary terms vanish under the stated BCs). One obtains after routine algebra

$$\int_{x_0}^{x_1} xU\, (xU_{xx} - xU_x)\, dx = -\int_{x_0}^{x_1} x^2 (U_x)^2\, dx \; + \; B[U],$$

where $B[U]$ comprises boundary terms which are zero under the assumed BCs (or are negative under certain dissipative BCs). Hence

$$\left(wU, D^\alpha U\right) = -\|xU_x\|^2_{L^2(\Omega)} \le 0.$$

For the classical time derivative $\alpha = 1$ we have

$$\frac{1}{2}\frac{d}{dt}\|U(\cdot, t)\|_w^2 = (wU, \partial_t U) = -\|xU_x\|^2_{L^2} \le 0,$$

so the weighted energy is nonincreasing and the continuous problem is energy-stable in the $\|\cdot\|_w$-norm.

For the fractional-in-time derivative D^α (Caputo) one uses the positive-definiteness of the fractional derivative in the Tarig domain. The key point is that the right-hand side is nonpositive, hence no source of energy growth is introduced by the spatial operator. Therefore the TPDTM iteration, when linearized, inherits boundedness provided the transform operator multiplier $\mathcal{O}$ is bounded (i.e. has finite norm b): in operator-norm form one obtains the contractivity requirement in the linear setting

$$b\|R\|_{w,\mathrm{op}} < 1,$$

where $\|R\|_{w,\mathrm{op}}$ is the operator norm induced by the weighted L^2_w-norm. When this holds, successive iterates decay and the iteration is stable.

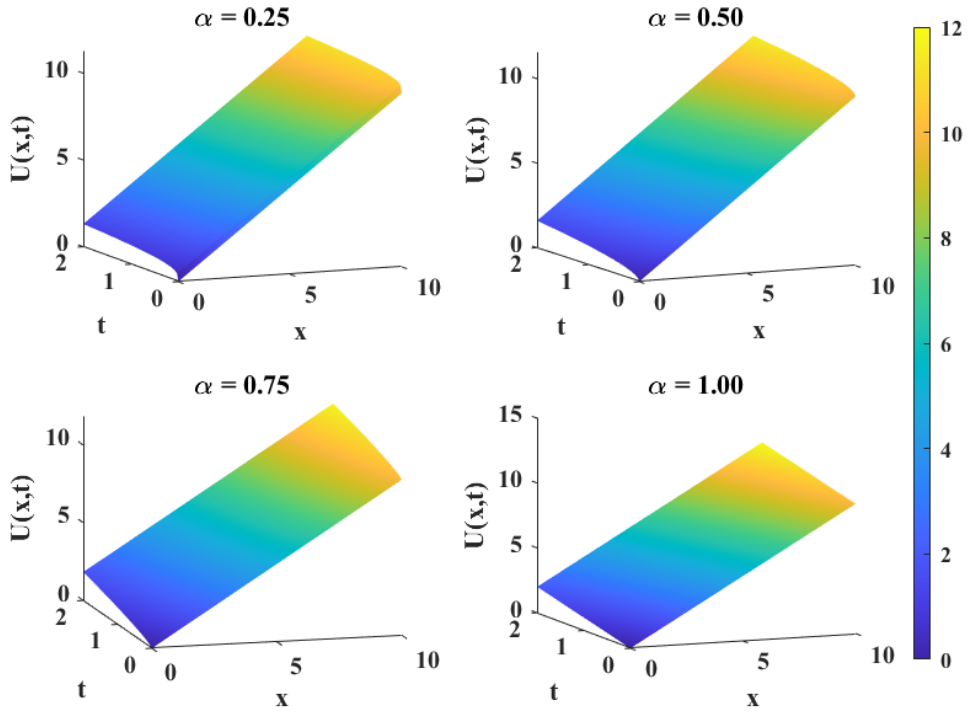

FIGURE 1. The TPDTM-generated approximate solutions for test example 1 across varying fractional order of α

Practical remarks.

- The assumption $x \geq x_0 > 0$ is natural for many Fokker–Planck-type problems; if the domain includes $x = 0$ one must handle the singularity at 0 (use a different weight or restrict to $x \in [x_0, x_1]$).
- Boundary terms arising in integration by parts must be handled consistently with the BCs used in the numerical experiments; for vanishing Dirichlet BCs the boundary terms drop out.
- The derivation shows the spatial operator is dissipative in the weighted energy sense (right-hand side ≤ 0), which is the main ingredient for stability.

4. Results and Discussion

We solve the time-fractional partial differential equation, namely the F-P equation, using the unique hybrid approach TPDTM. We calculate the approximate solution for four cases of the F-P equation by changing the drift coefficient $A(x)$ and the diffusion coefficient $B(x)$ from the nonlinear F-P equation (2). All calculations for this research were performed using MATLAB software. To evaluate the efficiency of TPDTM, we conduct a comparative analysis between TPDTM and

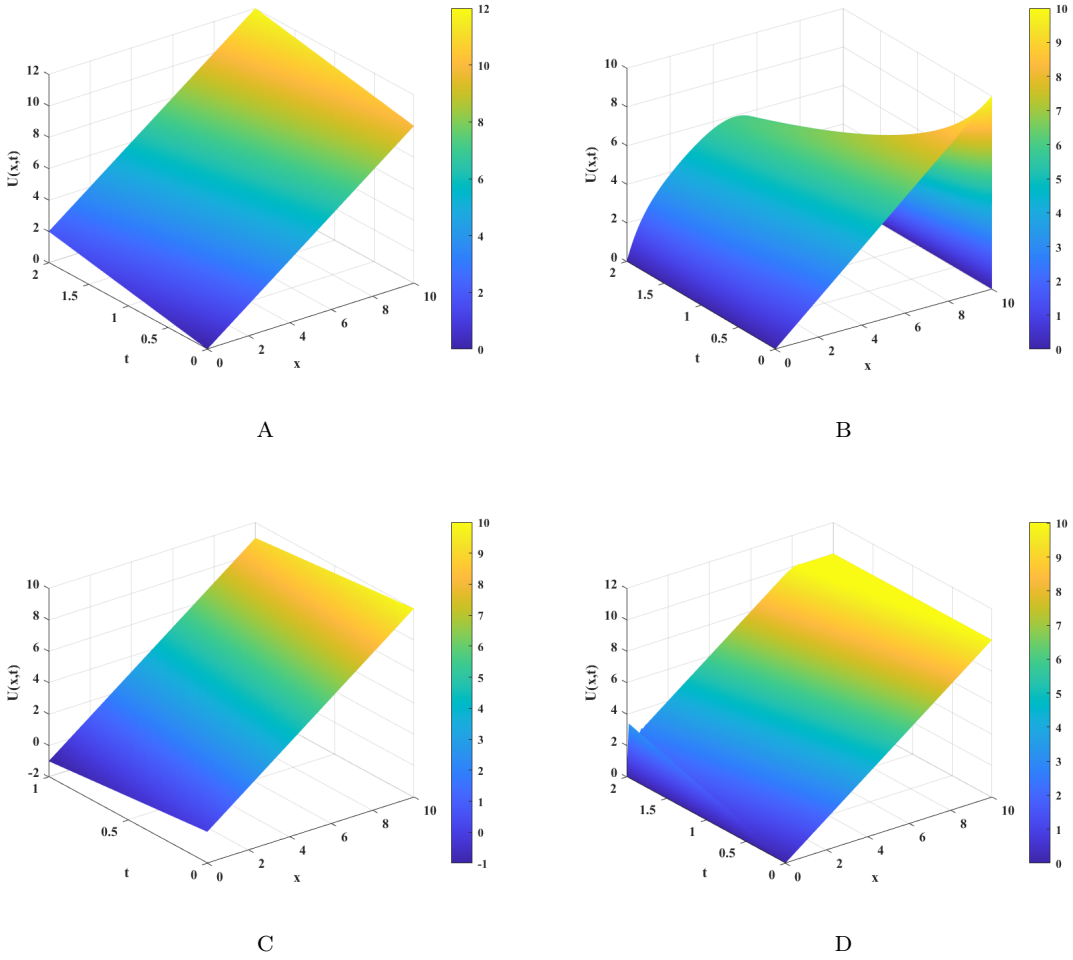

FIGURE 2. Plots of $U(x,t)$ Using (a) TPDTM, (b) FDM, (c) LADM, and (d) HPM of test example 1.

well-established numerical methods, including FDM, LADM, and HPM is made, and 2D/3D graphs and tables illustrate the results. Tables 1, 3, 5, and 7 represent the approximate numerical solution of the four cases of F-P equations for different values of fractional order α, and the graphical representation of Tables 1, 3, 5, and 7 are depicted in Figures 1, 3(a), 4, 6(a), 7, 9(a), and Figures 10, 12(a), respectively. Figures (2, 5, 8, and 11) denote the approximate numerical solution of the fractional differential equation of the four cases of F-P equations obtained by TPDTM, FDM, LADM, and HPM, respectively. Figures (2, 5, 8, and 11), it is obvious that a clear uniformity is observed in all numerical solutions generated by the TPDTM approach (2(a), 5(a), 8(a) and 11(a)) and LADM (2(c), 5(c), 8(c) and 11(c)). There is a similarity between solution obtained by FDM (5(b), and 8(b)) and HPM (5(d), and 8(d)). From Figures 3(b), 6(b), 9(b), and 12(b), it is clear

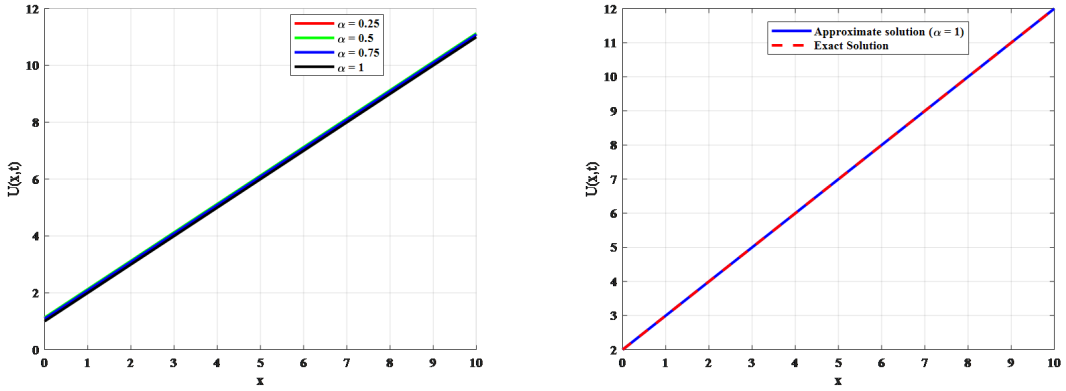

A B

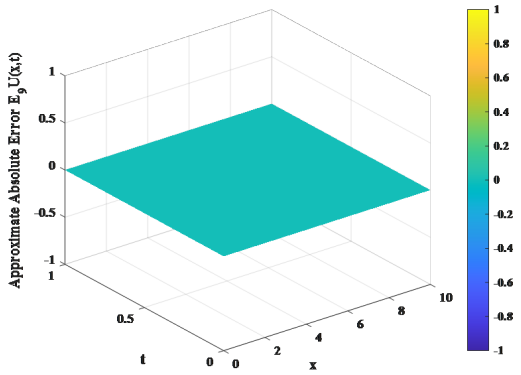

C

FIGURE 3. (a) Comparison between exact and TPDTM approximate solutions for test example 1, showing $U(x,t)$ versus x at $t = 1$ for fractional orders $\alpha = 0.25, 0.5, 0.75$, and 1 . (b) Detailed comparison of exact and approximate solutions at $\alpha = 1$. (c) $Absoluteerror = |Exact - Approximate|$, between the solutions

that the exact and approximate solutions of the fractional F-P equations of all four cases using TPDTM are in complete agreement. The maximum errors for each of the four different cases of the F-P equation for different values x provided in tables 2, 4, 6, and 8 offer deeper insight into the stability and convergence properties of the numerical method TPDTM. Using the concepts in subsection 2.5, from Tables 2, 4, 6, and 8, it is clear that an increase in n causes in a reduction in the value of error. This means the sequence $E_nU(x,t)$ is monotonically decreasing, and it is clear from Tables 2, 4, 6, and 8 that $E_kU(x,t)$ is bounded below, the sequence

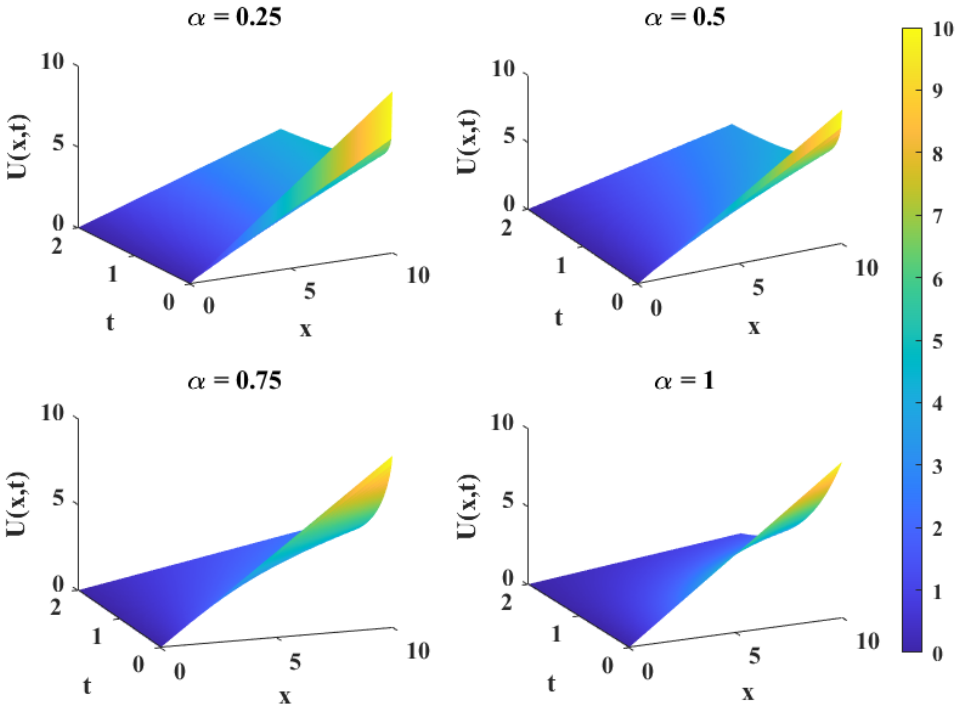

FIGURE 4. The TPDTM-generated approximate solutions for test example 2 across varying fractional order of α

TABLE 1. $U(x,t)$ corresponding to various values of α and x , at $t = 1$ of 1^{st} test example

x-value	$U(x,t)$ corresponding to various values of α			
	$\alpha = 0.25$	$\alpha = 0.5$	$\alpha = 0.75$	$\alpha = 1$
1	2.1033	2.1284	2.0881	2
2	3.1033	3.1284	3.0881	3
3	4.1033	4.1284	4.0881	4
4	5.1033	5.1284	5.0881	5
5	6.1033	6.1284	6.0881	6
6	7.1033	7.1284	7.0881	7
7	8.1033	8.1284	8.0881	8
8	9.1033	9.1284	9.0881	9
9	10.1033	10.1284	10.0881	10
10	11.1033	11.1284	11.0881	11

$E_nU(x,t)$ is a convergent sequence, demonstrates the approximate numerical solution using the TPDTM approach to the exact solution, and indicates the method of TPDTM converging well. Also, our work's remarkable achievement is that the error remains bounded without significant growth, demonstrating numerical stability.

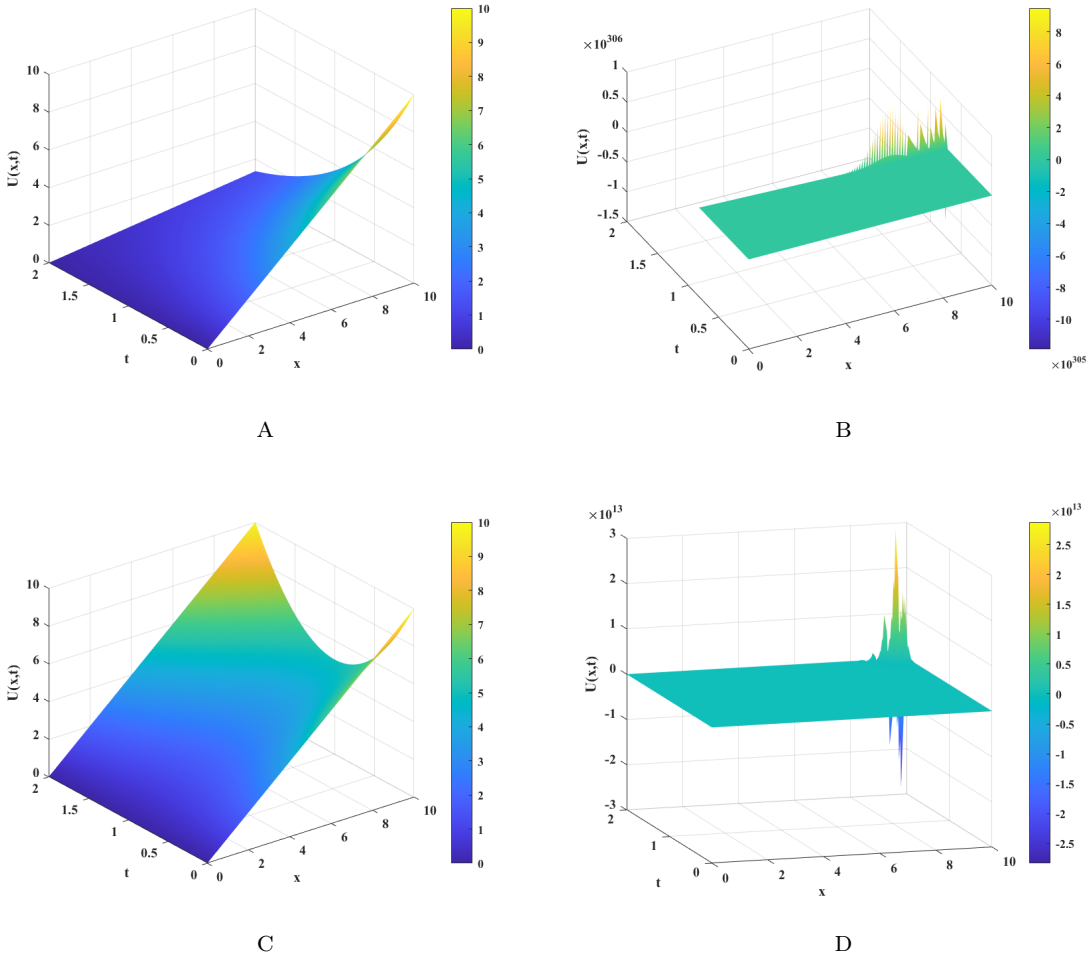

FIGURE 5. Plots of $U(x,t)$ Using (a) TPDTM, (b) FDM, (c) LADM, and (d) HPM of test example 2.

Figures 3(c), 6(c), 9(c), and 12(c) give the absolute error of the ninth term of the four different case series. Higher iteration counts yield progressively more accurate solutions, demonstrating the method's convergence properties.

5. Conclusions

The numerical solutions obtained through TPDTM show excellent agreement with the exact solution. The results clearly demonstrate that while TPDTM maintains simplicity in its approach, it delivers highly effective and accurate outcomes.The sequence of approximate solutions of time-fractional F-P equations (four different cases) converges to their exact solutions rapidly, indicating that the TPDTM is a strong and reliable algorithm. Compared with the existing well-known methods in

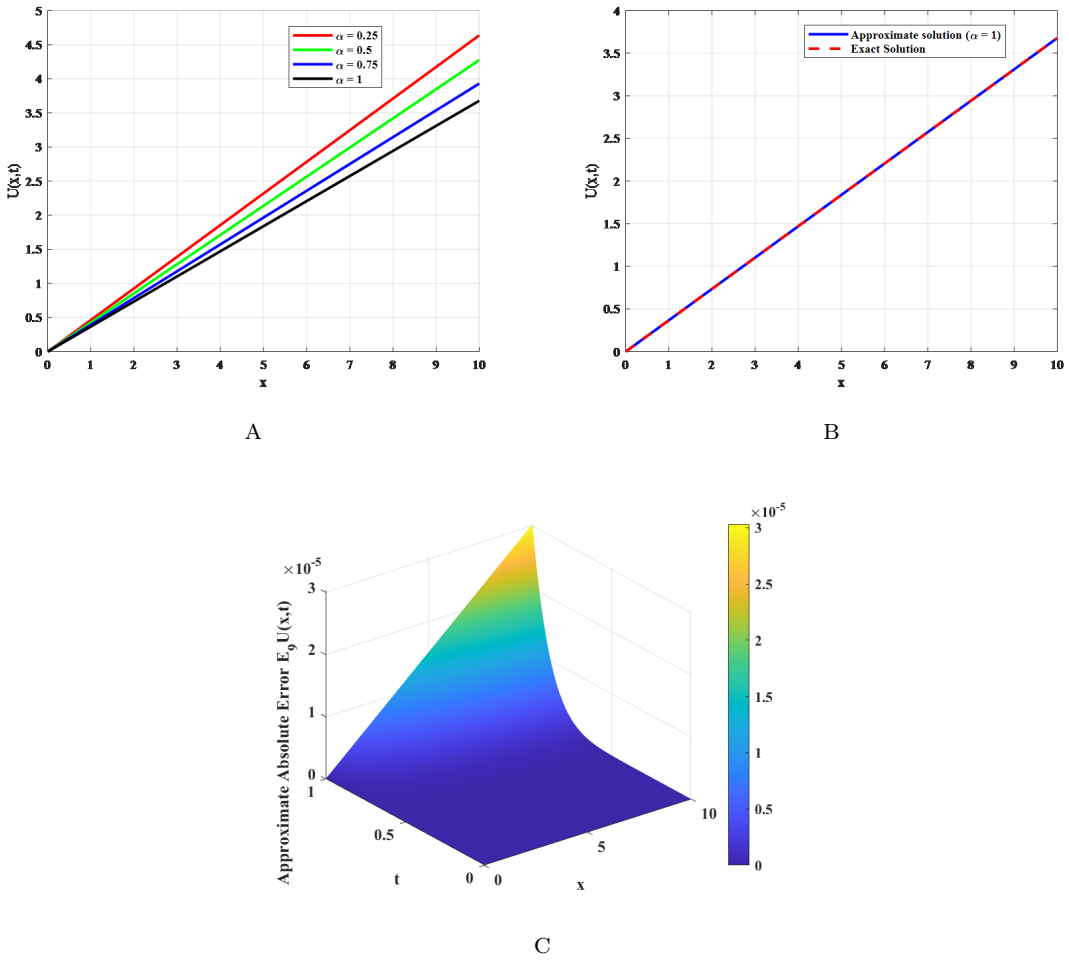

FIGURE 6. (a) Comparison between exact and TPDTM approximate solutions for test example 2, showing $U(x,t)$ versus x at $t = 1$ for fractional orders $\alpha = 0.25, 0.5, 0.75$, and 1 . (b) Detailed comparison of exact and approximate solutions at $\alpha = 1$. (c) Absolute error = |Exact-Approximate| between the solutions

the literature, the TPDTM does not require linearization, perturbation, discretization of variables, or other limiting assumptions. The computational time of this method is comparatively less. As a result, TPDTM emerges as an attractive alternative to conventional techniques, combining implementation simplicity with robust computational performance and reliability. This study highlights the potential of TPDTM as a robust and adaptable tool, providing a valuable contribution to fractional calculus and its applications in science, engineering, and technology.

TPDTM can be employed to model complex physical phenomena where memory effects, anomalous diffusion, and anomalous transport are significant, such as in

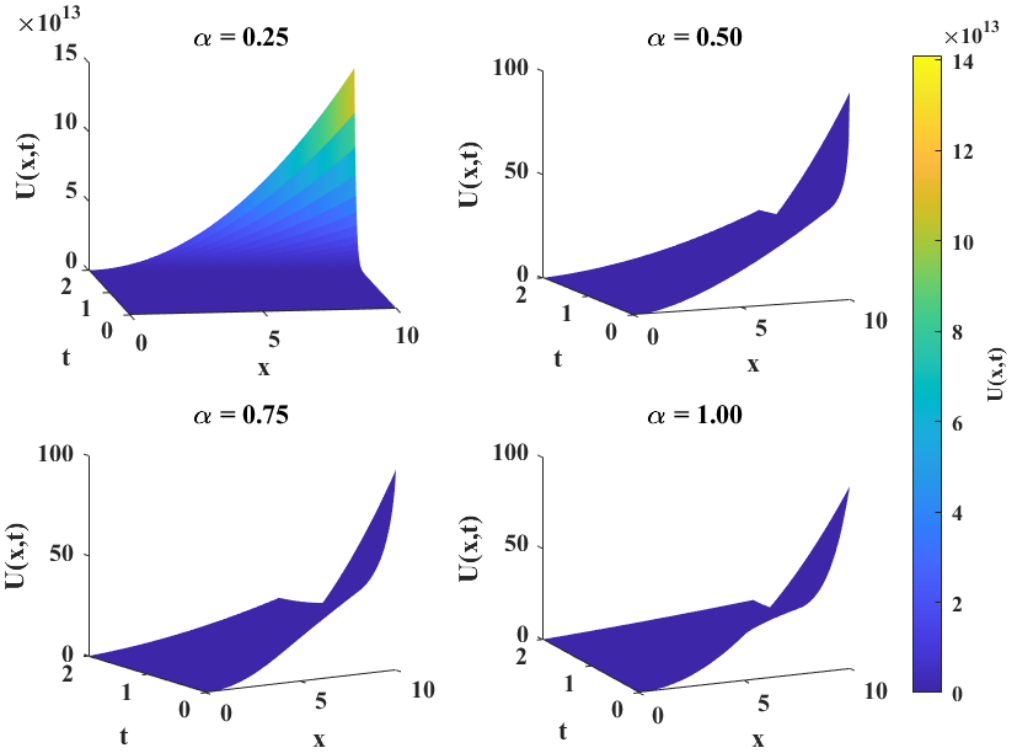

FIGURE 7. The TPDTM-generated approximate solutions for test example 3 across varying fractional order of α

TABLE 2. Absolute error analysis of $U(x,t)$ for test example 1, evaluated at $t = 1$ across various x and n values.

n	$E_n U(x,t)$ corresponding to different values of x					
	$x = 0$	$x = 2$	$x = 4$	$x = 6$	$x = 8$	$x = 10$
1	1	1	1	1	1	1
2	0	0	0	0	0	0
3	0	0	0	0	0	0
4	0	0	0	0	0	0
5	0	0	0	0	0	0
6	0	0	0	0	0	0
7	0	0	0	0	0	0
8	0	0	0	0	0	0
9	0	0	0	0	0	0

plasma dynamics, astrophysical flows, experimental fluid dynamics (particularly in wind tunnel experiments of shock tube studies), biomedical experiments, and non-equilibrium thermodynamics.

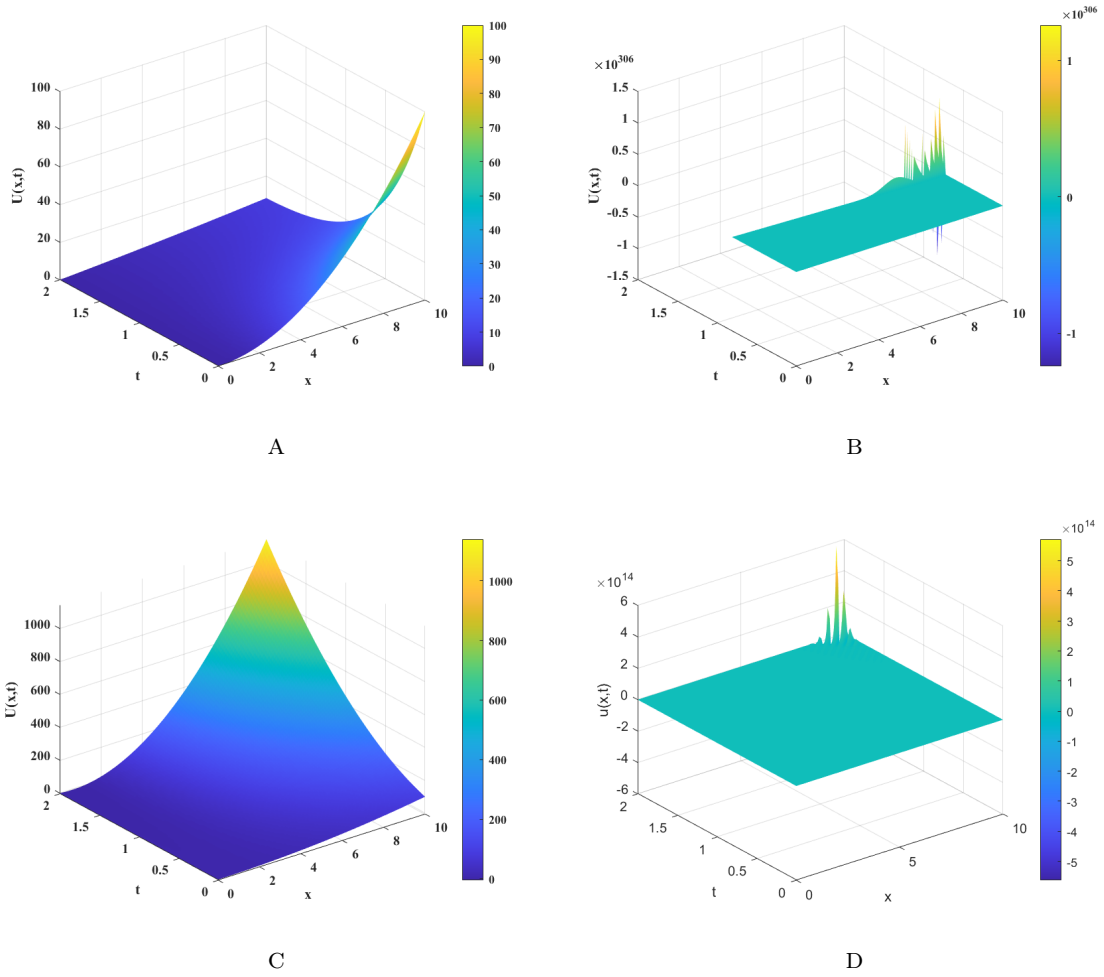

FIGURE 8. Plots of $U(x,t)$ Using (a) TPDTM, (b) FDM, (c) LADM, and (d) HPM of test example 3.

The TPDTM method is a potential tool for advancing simulations with real-time monitoring and control experiments in aerospace propulsion, combustion systems, microfluidics, and high-speed gas flows, where accurate and efficient numerical solutions of fractional-order models can improve system design and optimization under dynamic flow conditions. Additionally, TPDTM can be extended to multi-dimensional, nonlinear, coupled systems, enhancing its relevance in modelling real-world gas dynamics involving interactions with thermal, electromagnetic, or chemical processes.

TPDTM algorithms can be incorporated into numerical toolboxes for researchers and engineers dealing with fractional differential equations, providing a numerically stable and fast-converging alternative to traditional solvers, benefiting applications in environmental modeling, biomedical simulations (e.g., modeling airflow in lungs

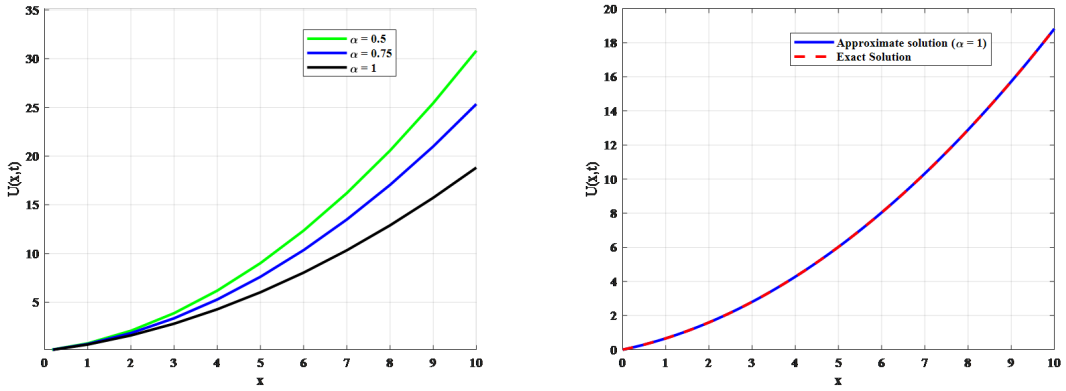

A B

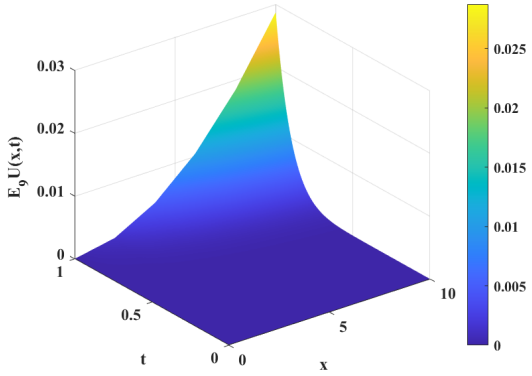

C

FIGURE 9. (a) Comparison between exact and TPDTM approximate solutions for test example 3, showing $U(x,t)$ versus x at $t = 1$ for fractional orders $\alpha = 0.25, 0.5, 0.75$, and 1 . (b) Detailed comparison of exact and approximate solutions at $\alpha = 1$. (c) Absolute error = |Exact-Approximate| between the solutions

or gas exchange systems with memory effects.), and intelligent control systems for fluid transport. Furthermore, hybrid models combining TPDTM with data-driven methods (e.g., neural networks or physics-informed machine learning) can enhance predictive accuracy in complex, real-time technological systems.

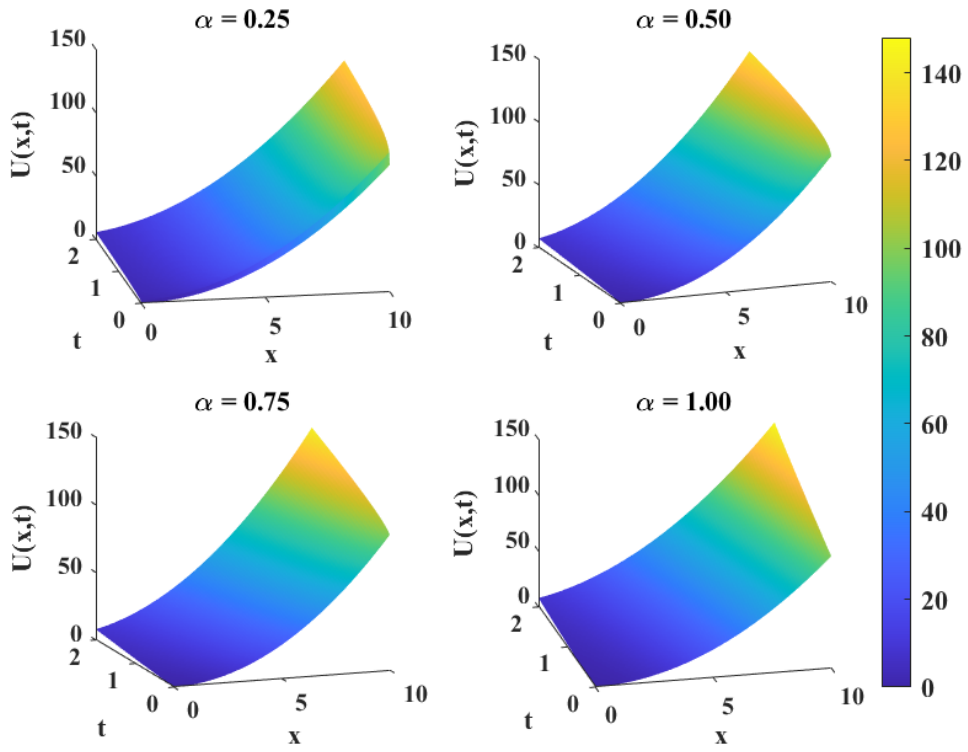

FIGURE 10. The TPDTM-generated approximate solutions for Test Example 4 across varying fractional order of α

TABLE 3. $U(x,t)$ corresponding to various values of α and x, at $t = 1$ of 2^{nd} test example 2.

x-value	$U(x,t)$ corresponding to various values of α			
	$\alpha = 0.25$	$\alpha = 0.5$	$\alpha = 0.75$	$\alpha = 1$
1	0.46385	0.42758	0.39311	0.36788
2	0.92771	0.85517	0.78622	0.73576
3	1.3916	1.2828	1.1793	1.1036
4	1.8554	1.7103	1.5724	1.4715
5	2.7831	2.1379	1.9655	1.8394
6	2.7831	2.5655	2.3586	2.5752
7	3.247	2.9931	2.7518	2.5752
8	3.7108	3.4207	93.1449	2.943
9	4.1747	3.8483	3.538	3.3109
10	4.6385	4.2758	3.9311	3.6788

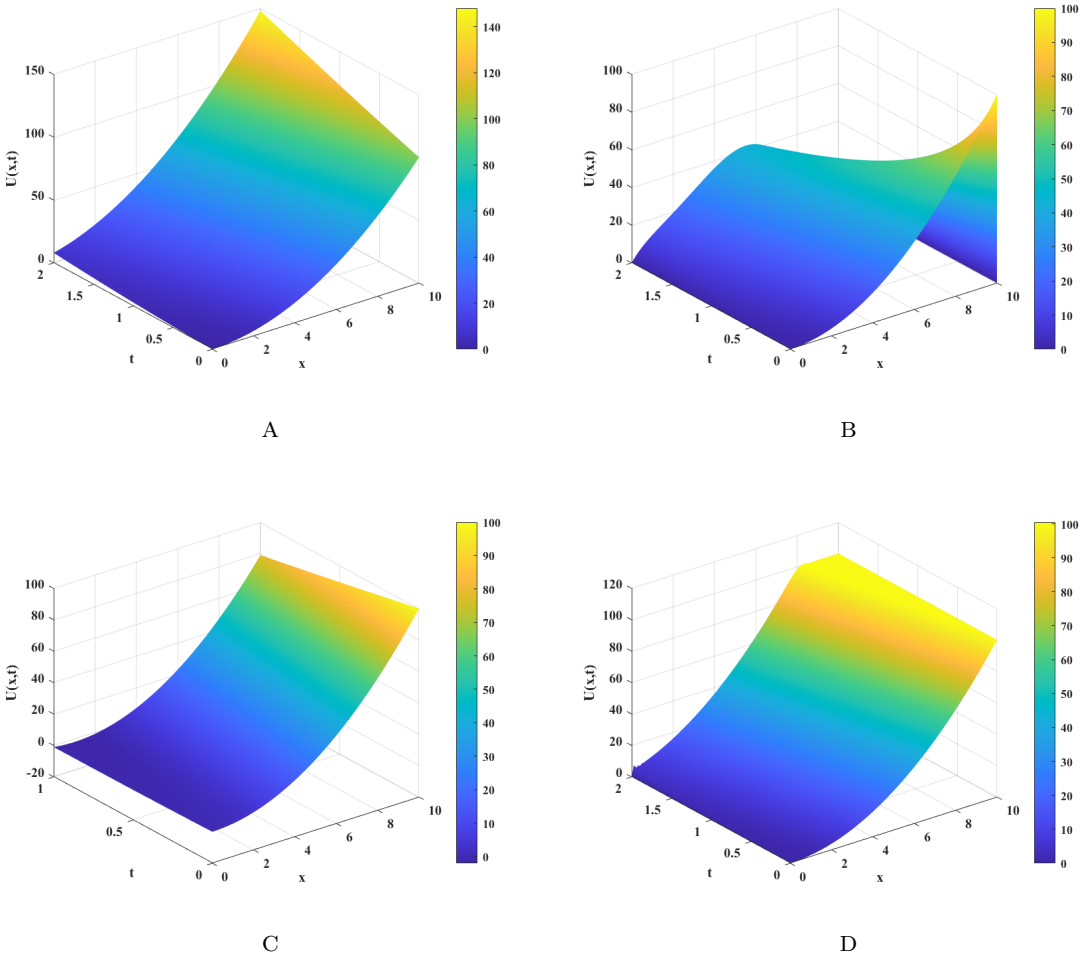

FIGURE 11. Plots of $U(x,t)$ Using (a) TPDTM, (b) FDM, (c) LADM, and (d) HPM of test example 4 .

TABLE 4. Absolute error analysis of $U(x,t)$ for test example 2, evaluated at $t = 1$ across various x and n values.

n	$E_nU(x,t)$ corresponding to different values of x					
	$x = 0$	$x = 2$	$x = 4$	$x = 6$	$x = 8$	$x = 10$
1	0	1	2	3	4	5
2	0	0.33333	0.66667	1	1.3333	1.6667
3	0	0.083333	0.16667	0.25	0.33333	0.41667
4	0	0.016667	0.033333	0.05	0.066667	0.083333
5	0	0.0027778	0.0055556	0.0083333	0.011111	0.013889
6	0	0.00039683	0.00079365	0.0011905	0.0015873	0.0019841
7	0	4.9603e-05	9.9206e-05	0.00014881	0.00019841	0.00024802
8	0	5.5115e-06	1.1023e-05	1.6534e-05	2.2046e-05	2.7557e-05
9	0	5.5115e-07	1.1023e-06	1.6534e-06	2.2046e-06	2.7557e-06

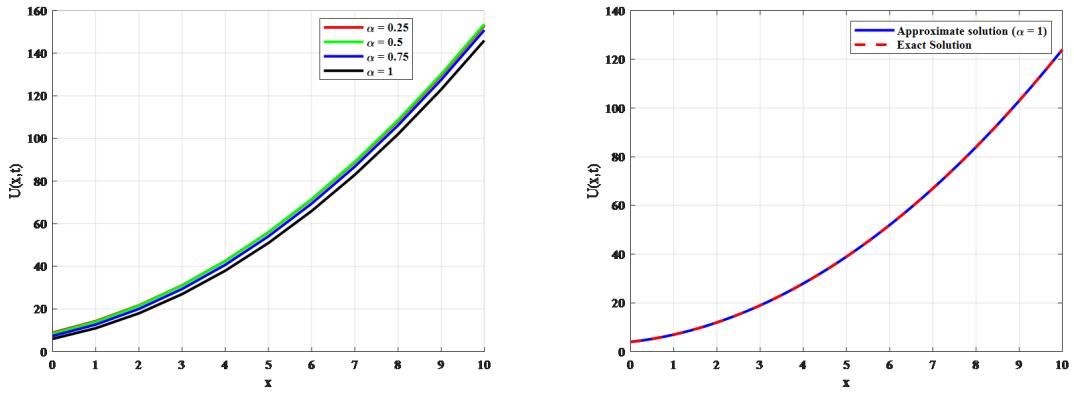

A B

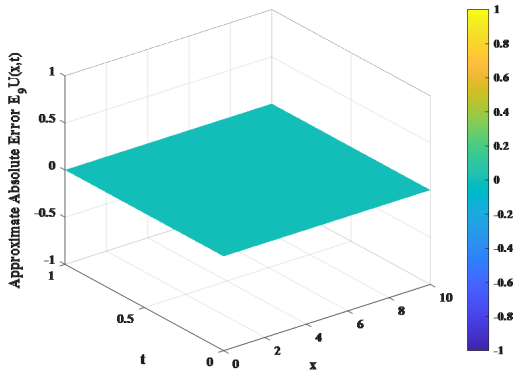

C

FIGURE 12. (a) Comparison between exact and TPDTM approximate solutions for test example 4, showing $U(x,t)$ versus x at $t = 1$ for fractional orders $\alpha = 0.25, 0.5, 0.75$, and 1 . (b) Detailed comparison of exact and approximate solutions at $\alpha = 1$. (c) Absolute error = |Exact-Approximate| between the solutions

TABLE 5. $U(x,t)$ corresponding to various values of α and x, at $t=1$ of 3^{rd} test example

x	$U(x,t)$ corresponding to various values of α			
	$\alpha=0.25$	$\alpha=0.5$	$\alpha=0.75$	$\alpha=1$
1	38483	0.78274	0.71515	0.66382
2	1.5393e+05	2.0763	1.8345	1.5983
3	3.4635e+05	3.8806	3.3579	2.8035
4	6.1573e+05	6.1957	5.2855	5.2855
5	9.6207e+05	9.0216	7.6173	6.0258
6	1.3854e+06	12.358	10.353	8.043
7	1.8857e+06	16.206	13.493	10.331
8	2.4629e+06	20.564	17.038	12.889
9	3.1171e+06	25.433	20.986	15.718
10	3.8483e+06	30.813	25.339	18.818

TABLE 6. Absolute error analysis of $U(x,t)$ for test example 3, evaluated at $t=1$ across various x and n values.

n	$E_nU(x,t)$ corresponding to different values of x					
	$x=0$	$x=2$	$x=4$	$x=6$	$x=8$	$x=10$
1	0	14	44	90	152	230
2	0	0.66667	12	34	66.667	110
3	0	4.8333	15	30.5	51.333	77.5
4	0	0.36667	2.8667	7.5	14.267	23.167
5	0	0.52778	1.7667	3.7167	6.3778	9.75
6	0	0.06746	0.3381	0.8119	1.4889	2.369
7	0	0.031052	0.1129	0.24554	0.42897	0.66319
8	0	0.0048391	0.020966	0.04838	0.087081	0.13707
9	0	0.0012291	0.0047156	0.01046	0.018461	0.02872

TABLE 7. $U(x,t)$ corresponding to various values of $\alpha$and x, at $t=1$ of 4^{th} test example.

x	$U(x,t)$ corresponding to various values of α			
	$\alpha=0.25$	$\alpha=0.5$	$\alpha=0.75$	$\alpha=1$
0	8.9266	8.5135	7.3613	6
1	14.34	14.027	12.714	11
2	21.753	21.541	20.066	18
3	31.166	31.054	29.418	27
4	42.579	42.568	40.77	38
5	55.992	56.081	54.123	51
6	71.405	71.595	69.475	66
7	88.818	89.108	86.827	83
8	108.23	108.62	106.18	102
9	129.64	130.14	127.53	123
10	153.06	153.65	150.88	146

TABLE 8. Absolute error analysis of $U(x,t)$ for test example 4, evaluated at $t = 1$ across various x and n values

n	$E_nU(x,t)$ corresponding to different values of x					
	$x=0$	$x=2$	$x=4$	$x=6$	$x=8$	$x=10$
1	0	4	16	36	64	100
2	2	6	10	14	18	22
3	1	1	1	1	1	1
4	0	0	0	0	0	0
5	0	0	0	0	0	0
6	0	0	0	0	0	0
7	0	0	0	0	0	0
8	0	0	0	0	0	0
9	0	0	0	0	0	0

TABLE 9. Comparative analysis from the existing literature

Reference paper	FDM (Chen et al. (2009))[17]	LADM (Zhang et al. (2024))[76]	HPM (Yildirim and Ahmet (2010)) [75]	Present Study
Result	In this study, they described and illustrated three finite difference implicit approximations for the fractional F-P equation in a bounded domain. They have demonstrated the unconditional stability and convergence of these finite difference approximations. They concluded that other fractional partial differential equations can be resolved using these methods.	This research used the LADM to obtain an approximate solution to the FFPE and TFCBBEs. The errors between the results and the exact solutions are compared using a variety of numerical examples and graphs. The findings demonstrate that LADM is a straightforward and efficient mathematical method for creating approximations of nonlinear time-space fractional equation solutions in this work.	The F-P equation was successfully solved in this work using the HPM. This approach uses only the initial condition to discover exact solutions to equations. They concluded that, compared to conventional methods, the method requires much less computational work. It is demonstrated that HPM is a highly accurate, cost-effective, and quickly convergent method for resolving nonlinear differential equations.	The numerical solutions obtained through TPDTM show excellent agreement with the exact solution. These results demonstrate that TPDTM offers a straightforward yet highly effective approach, delivering precise and accurate outcomes. Consequently, TPDTM emerges as a practical, computationally efficient, and reliable method that is remarkably easy to implement. Its advantages make it an attractive alternative to existing well-established methods in the research community.

Acknowledgment

The authors gratefully acknowledge the financial support provided by the University Grants Commission (UGC), New Delhi, India, under the Savitribai Jyotirao Phule Fellowship for Single Girl Child (SJSGC) scheme. [F. No.82-7/2022(SA-III)]. Also thank to the reviewers for their valuable suggestions and comments that improved the quality of paper.

References

[1] P. S. Acioli, F. A. Xavier, and D. M. Moreira, *Mathematical model using fractional derivatives applied to the dispersion of pollutants in the planetary boundary layer*, Boundary-Layer Meteorol., **170** (2019), 285–304.

[2] R. Agarwala, D. Baleanu, J. J. Nieto, D. F. M. Torres, and Y. Zhou, *A survey on fuzzy fractional differential and optimal control nonlocal evolution equations*, J. Comput. Appl. Math., **339** (2017), 3–29.

[3] M. A. Al-Jawary, *An efficient iterative method for solving the Fokker–Planck equation*, Results Phys., **6** (2016), 985–991.

[4] K. Athira, D. Narasimhulu, and P. S. Brahmanandam, *Numerical solutions of time-fractional NWS and Burger's equations using the Tarig Projected Differential Transform Method (TPDTM)*, Contemp. Math., **6** (2025), 2907–2928.

[5] K. Aruna, N. I. Okposo, K. Raghavendar, and M. Inc, *Analytical solutions for the Noyes Field model of the time fractional Belousov Zhabotinsky reaction using a hybrid integral transform technique*, Sci. Rep., **14** (2024), 25015.

[6] Z. Ayati, J. Biazar, and S. Ebrahimi, *Analytical approach to fractional Fokker–Planck equations by new homotopy perturbation method*, J. Math. Comput. Sci., **9** (2014), 426–437.

[7] M. Ayata and O. Özkan, *An analytical solution to conformable fractional Fokker–Planck equation*, Karaelmas Fen Müh. Derg., **12** (2022), 9–14.

[8] M. Bagyalakshmi and G. SaiSundarakrishnan, *Tarig projected a differential transform method to solve fractional nonlinear partial differential equations*, Bol. Soc. Paran. Mat., **38** (2020), 23–46.

[9] Y. A. Berezin, V. N. Khudick, and M. S. Pekker, *Conservative finite-difference schemes for the Fokker–Planck equation not violating the law of an increasing entropy*, J. Comput. Phys., **69** (1987), 163–174.

[10] J. Biazar, K. Hosseini, and P. Gholamin, *Homotopy perturbation method Fokker-Planck equation*, Int. Math. Forum, **3** (2008), 945–954.

[11] C. Buet and S. Cordier, *Conservative and entropy decaying numerical scheme for the isotropic Fokker–Planck–Landau equation*, J. Comput. Phys., **145** (1998), 228–245.

[12] C. Buet, S. Cordier, P. Degond, and M. Lemou, *Fast algorithms for numerical, conservative, and entropy approximations of the Fokker–Planck–Landau equation*, J. Comput. Phys., **133** (1997), 310–322.

[13] C. Buet and S. Cordier, *Numerical analysis of conservative and entropy schemes for the Fokker–Planck–Landau equation*, SIAM J. Numer. Anal., **36** (1999), 953–973.

[14] C. Buet, S. Dellacherie, and R. Sentis, *Numerical solution of an ionic Fokker–Planck equation with electronic temperature*, SIAM J. Numer. Anal., **39** (2001), 1219–1253.

[15] M. Caputo, *Elasticitae Dissipazione, Zanichelli, Bologna*, SIAM Journal on Numerical Analysis, Italy, (1969).

[16] D. Chen, Y. Chen, and D. Xue, *Three fractional-order TV-L2 models for image denoising*, J. Comput. Inf. Syst., **9**(12) (2013), 4773–4780.

[17] S. Chen, F. Liu, P. Zhuang, and V. Anh, *Finite difference approximations for the fractional Fokker–Planck equation*, Appl. Math. Model., **33** (2009), 256–273.

[18] P. Cui and H. K. Jassim, *Local fractional Sumudu decomposition method to solve fractal PDEs arising in mathematical physics*, Fractals, **32** (2024), 1–7.

[19] S. Das, *Analytical solution of a fractional diffusion equation by variational iteration method*, Comput. Math. Appl., **57**(3) (2009), 483–487.

[20] P. Degond and B. Lucquin-Desreux, *The Fokker–Planck asymptotics of the Boltzmann collision operator in the Coulomb case*, Math. Models Methods Appl. Sci., **2** (1992), 167–182.

[21] M. Dehghan and M. Tatari, *The use of He's variational iteration method for solving a Fokker–Planck equation*, Phys. Scr., **74** (2006), 310.

[22] W. H. Deng, *Generalized synchronization in fractional order systems*, Phys. Rev. E, **75** (2007), 056201.

[23] W. Deng, *Finite element method for the space and time fractional Fokker–Planck equation*, SIAM J. Numer. Anal., **47** (2009), 204–226.

[24] W. H. Deng and J. H. Li, *Design of multi-directional multi-scroll chaotic attractors based on fractional differential systems via switching control*, Chaos, **16** (2006), 043120.

[25] A. N. Drozdov and M. Morillo, *Solution of nonlinear Fokker-Planck equations*, Phys. Rev. E, **54** (1996),931.

[26] R. S. Dubey, B. S. T. Alkahtani, and A. Atangana, *Analytical solution of space-time fractional Fokker-Planck equation by Homotopy Perturbation Sumudu Transform Method*, Math. Probl. Eng., **2015** (2025), 780929.

[27] T. M. Elzaki and S. M. Elzaki, *The new integral transform "Tarig Transform" properties and applications to differential equations*, Elixir Int. J., **38** (2011), 4239–4242.

[28] V. S. Erturk and S. Momani, *Solving systems of fractional differential equations using differential transform method*, J. Comput. Appl. Math., **215**(1) (2008), 142–151.

[29] J. Fok, B. Guo, and T. Tang, *Combined Hermite spectral-finite difference method for the Fokker-Planck equation*, Math. Comput., **71** (2002), 1497–1528.

[30] E. A. Gonzalez and I. Petras, *Advances in fractional calculus: Control and signal processing applications*, Proc. 16th Int. Carpathian Control Conf. (ICCC), IEEE, 2025.

[31] P. F. Han, W.X. Ma, R.S. Ye, and Y. Zhang, *Inverse scattering transform for the defocusing–defocusing coupled Hirota equations with non-zero boundary conditions: Multiple double-pole solutions*, Physica D, **471** (2025), 134434.

[32] P. F. Han, R.-S. Ye, and Y. Zhang, *Inverse scattering transform for the coupled Lakshmanan–Porsezian–Daniel equations with non-zero boundary conditions in optical fiber communications*, Math. Comput. Simul., **232** (2025), 483–503.

[33] P.F. Han and Y. Zhang, *Superposition behavior of the lump solutions and multiple mixed function solutions for the (3+1)-dimensional Sharma–Tasso–Olver-like equation*, Eur. Phys. J. Plus, **139** (2024), 157.

[34] P. F. Han and Y. Zhang, *Investigation of shallow water waves near the coast or in lake environments via the KdV–Calogero–Bogoyavlenskii–Schiff equation*, Chaos Solitons Fractals, **184** (2024), 115008.

[35] P. F. Han, Y. Zhang, and C.-H. Jin, *Novel evolutionary behaviors of localized wave solutions and bilinear auto-Bäcklund transformations for the generalized (3+1)-dimensional Kadomtsev–Petviashvili equation*, Nonlinear Dyn., **111** (2023), 8617–8636.

[36] P. F. Han, K. Zhu, F. Zhang, W. X. Ma, and Y. Zhang, *Inverse scattering transform for the fourth-order nonlinear Schrödinger equation with fully asymmetric non-zero boundary conditions*, Chin. J. Phys. **96** (2025), 577–602.

[37] H. Hanif, *A computational approach for boundary layer flow and heat transfer of fractional Maxwell fluid*, Math. Comput. Simul., **191** (2022), 1–13.

[38] O. Heaviside, *Electromagnetic Theory*, Chelsea, New York, 1971.

[39] A. A. Hemeda and E. E. Eladdad, *New iterative methods for solving Fokker–Planck equation*, Math. Probl. Eng., **2018** (2018), 6462174.

[40] C. Hirsch, *Numerical Computation of Internal and External Flows: The Fundamentals of Computational Fluid Dynamics*, Elsevier, 2007.

[41] M. Ichise, Y. Nagayanagi, and T. Kojima, *An analog simulation of non-integer order transfer function for analysis of electrode processes*, J. Electroanal. Chem., **33** (1971), 253–265.

[42] M. A. Jafari and A. Aminataei, *Application of homotopy perturbation method in the solution of Fokker–Planck equation*, Phys. Scr., **80** (2009), 055001.

[43] G. Jumarie, *Fractional Brownian motions via random walk in the complex plane and via fractional derivative*, Chaos Solitons Fractals, **22** (2004), 907–925.

[44] B. Jang, *Solving linear and nonlinear initial value problems by the projected differential transform method*, Comput. Phys. Commun., **181** (2010), 845–854.

[45] Y. Li and N. Sun, *Numerical solution of fractional differential equations using the generalized block pulse operational matrix*, Comput. Math. Appl., **62**(3) (2011), 1046–1054.

[46] Y. Liu, *Approximate solutions of fractional nonlinear equations using homotopy perturbation transformation method*, Abstr. Appl. Anal., **2012** (2012), Article ID 752869, 14 pages.

[47] A. Loverro, *Fractional Calculus: History, Definitions, and Applications for the Engineer*, Technical Report, Department of Aerospace and Mechanical Engineering, University of Notre Dame, 2004.

[48] Y. Kamitani and I. Matsuba, *Self-similar characteristics of neural networks based on Fokker–Planck equation*, Chaos Solitons Fractals, **20** (2004), 329–335.

[49] R. C. Koeller, *Application of fractional calculus to the theory of viscoelasticity*, J. Appl. Mech., **51** (1984), 229–307.

[50] S. Kumar, *Numerical computation of time-fractional Fokker–Planck equation arising in solid state physics and circuit theory*, Z. Naturforsch. A, **68** (2013), 777–784.

[51] P. Kumar and S. Narayanan, *Solution of Fokker-Planck equation by finite element and finite difference methods for nonlinear systems*, Sādhanā, **31** (2006), 445–461.

[52] M. Lakestani and M. Dehghan, *Numerical solution of Fokker–Planck equation using the cubic B-spline scaling functions*, Numer. Methods Partial Differ. Equ., **25** (2009), 418–429.

[53] D. Looker and P. K. Banerji, *Fractional Tarig transforms and Mittag-Leffler Function*, Bol. Soc. Parana. Mat., **35** (2017), 83–92.

[54] R. Y. Magin, Y. Sagher, and S. Boregowda, *Application of fractional calculus in modeling and solving the bioheat equation*, WIT Trans. Ecol. Environ., **73** (2004).

[55] F. Mainardi, *Fractional Calculus and Waves in Linear Viscoelasticity: An Introduction to Mathematical Models*, World Scientific, 2010.

[56] B. Mandelbrot, *Some noises with 1/f spectrum, a bridge between direct current and white noise*, IEEE Trans. Inf. Theory, **13** (1967), 289–298.

[57] S.-L. Mei and D.-H. Zhu, *Interval Shannon wavelet collocation method for fractional Fokker–Planck equation*, Adv. Math. Phys., **2013** (2013), 821820.

[58] A. S. Mohamed, A. M. S. Mahdy, and A. H. Mtawa, *Approximate analytical solution to a time-fractional Fokker–Planck equation*, Bothalia, **45** (2015), 57–69.

[59] C. A. Monje, Y. Q. Chen, B. M. Vinagre, D. Xue, and V. Feliu, *Fractional-Order Systems and Controls*, Springer, 2010.

[60] I. Naâ s and S. Kessentini, *GSA improvement via the von Neumann stability analysis*, Natural Comput., **20** (2021), 471–511.

[61] M. Y. Ongun, *The Laplace Adomian decomposition method for solving a model for HIV infection of CD4+ cells*, Math. Comput. Model., **53**(5-6) (2011), 597–603.

[62] V. Palleschi and M. De Rosa, *Numerical solution of the Fokker–Planck equation. II. Multidimensional case*, Phys. Lett. A, **163** (1992), 381–391.

[63] K. Pavani, K. Raghavendran, and K. Aruna, *Solitary wave solutions of the time fractional Benjamin Bona Mahony Burger equation*, Sci. Rep., **14** (2024), 14596,

[64] A. S. Ravi Kanth, K. Aruna, and K. Raghavendar, *Natural transform decomposition method for the numerical treatment of the time fractional Burgers-Huxley equation*, Numer. Methods Partial Differ. Equ., **39** (2023), 2690–2718.

[65] S. G. Samko, *Fractional Integrals and Derivatives, Theory and Applications*, Gordon and Breach Science, 1993.

[66] B. Sepehrian and M. K. Radpoor, *Solving the Fokker–Planck equation via the compact finite difference method*, Comput. Methods Differ. Equ., **8** (2020), 493–504.

[67] M. Shoucri, Y. Peysson, and I. Shkarofsky, *Numerical solution of the Fokker–Planck equation: A fast and accurate algorithm*, Phys. Lett. A, **146** (1990), 378–386.

[68] J. Singh, H. K. Jassim, D. Kumar, and V. P. Dubey, *Fractal dynamics and computational analysis of local fractional Poisson equations arising in electrostatics*, Commun. Theor. Phys., **75** (2023), 125002.

[69] M. Tatari, M. Dehghan, and M. Razzaghi, *Application of the Adomian decomposition method for the Fokker–Planck equation*, Math. Comput. Model., **45** (2007), 639–650.

[70] Y. Wang, L. Liu, X. Zhang, and Y. Wu, *Positive solutions of an abstract fractional semipositone differential system model for bioprocesses of HIV infection*, Appl. Math. Comput., **258** (2015), 312—324.

[71] J. L. Wu, *A wavelet operational method for solving fractional partial differential equations numerically*, Appl. Math. Comput., **214**(1) (2009), 31–40.

[72] Y. Xu, F. Y. Ren, J. R. Liang, and W. Y. Qiu, *Stretched Gaussian asymptotic behavior for fractional Fokker–Planck equation on fractal structure in external force fields*, Chaos Solitons Fractals, **20** (2004), 581–586.

[73] Y. Xu, H. Zhang, Y. Li, K. Zhou, Q. Liu, and J. Kurths, *Solving Fokker–Planck equation using deep learning*, Chaos, **30**(1) (2020).

[74] Q. Yang, F. Liu, and I. Turner, *Computationally efficient numerical methods for time-and space-fractional Fokker–Planck equations*, Phys. Scr., **2009** (2009), 014026.

[75] A. Yıldırım, *Application of the homotopy perturbation method for the Fokker–Planck equation*, Int. J. Numer. Methods Biomed. Eng., **26** (2010), 1144–1154.

[76] Y. Zhang and L. Wang, *Application of Laplace Adomian decomposition method for fractional Fokker–Planck equation and time fractional coupled Boussinesq–Burger equations*, Eng. Comput., **41**(4) (2024), 793–818.

[77] Z. Zhao and C. Li, *A numerical approach to the generalized nonlinear fractional Fokker–Planck equation*, Comput. Math. Appl., **64** (2012), 3075–3089.

[78] M. X. Zhou, A. R. Kanth, K. Aruna, K. Raghavendar, H. Rezazadeh, M. Inc, and A. A. Aly, *Numerical solutions of time fractional Zakharov-Kuznetsov equation via Natural Transform Decomposition method with non-singular kernel derivatives*, J. Funct. Spaces, **2021**(1) (2021), 9884027.

[79] F. Zhou and X. Xu, *The third kind Chebyshev wavelets collocation method for solving the time-fractional equation*, Appl. Math. Comput., **280** (2016), 11–29.
[80] P. Zhuang, F. Liu, V. Anh, and I. Turner, *Numerical treatment for the fractional Fokker–Planck equation*, ANZIAM J., **48** (2006), 759–774.
[81] M. P. Zorzano, H. Mais, and L. Vazquez, *Numerical solution of two-dimensional Fokker–Planck equations*, Appl. Math. Comput., **98** (1999), 109–117.
[82] S. Zubair, N. I. Chaudhary, Z. A. Khan, and W. Wang, *Momentum fractional LMS for power signal parameter estimation*, Signal Process., **142** (2018), 441–449.

Appendix

Tarig transform of the derivative of Caputo derivative. The Tarig transform of the derivative of Caputo derivative is defined as

$$T\left[D^{\alpha}f(t)\right] = F^{\alpha}(\vartheta) = \frac{1}{\vartheta^{2\alpha}}F(\vartheta) - \sum_{i=1}^{n}\vartheta^{2(i-\alpha)-1}f^{(i-1)}(0).$$

Proof. We have

$$T[f(t)] = \frac{1}{\vartheta}\int_0^{\infty} e^{-t/\vartheta^2} f(t)\,dt, \quad \vartheta \neq 0,$$

and

$$D^{\alpha}f(t) = \frac{1}{\Gamma(m-\alpha)}\int_a^t \frac{f^{(m)}(\tau)}{(t-\tau)^{\alpha-m+1}}\,d\tau,$$

then

$$T[D^{\alpha}f(t)] = \frac{1}{\vartheta}\int_0^{\infty} e^{-t/\vartheta^2}\left(D^{\alpha}f(t)\right)dt$$

$$= \frac{1}{\vartheta}\int_0^{\infty} e^{-t/\vartheta^2}\left[\frac{1}{\Gamma(m-\alpha)}\int_a^t \frac{f^{(m)}(\tau)}{(t-\tau)^{\alpha-m+1}}\,d\tau\right]dt, \quad \vartheta \neq 0.$$

Using the Gamma function property and rearranging, we obtain

$$T[D^{\alpha}f(t)] = \frac{\vartheta^{2(m-\alpha)}}{\vartheta}\int_0^{\infty} e^{-t/\vartheta^2}\left[\frac{1}{\vartheta}\int_0^{\infty} e^{-t/\vartheta^2} f^{(m)}(t)\,dt\right]dt. \tag{33}$$

From equation (33), let

$$I = \int_0^{\infty} e^{-t/\vartheta^2} f^{(m)}(t)\,dt.$$

Integrating by parts, we get

$$I = -f^{(m-1)}(0) + \frac{1}{\vartheta^2}\int_0^{\infty} e^{-t/\vartheta^2} f^{(m-1)}(t)\,dt. \tag{34}$$

From equation (34), set

$$I_1 = \int_0^{\infty} e^{-t/\vartheta^2} f^{(m-1)}(t)\,dt.$$

Integrating, we find

$$I_1 = -f^{(m-2)}(0) + \frac{1}{\vartheta^2}\int_0^\infty e^{-t/\vartheta^2} f^{(m-2)}(t)\,dt.$$

Continuing in this way and combining all I_i terms, at the $(m-1)^{\text{th}}$ step, we obtain

$$\begin{aligned} I = &- f^{(m-1)}(0) - \frac{1}{\vartheta^2} f^{(m-2)}(0) - \frac{1}{\vartheta^2 \cdot 2} f^{(m-3)}(0) - \cdots - \frac{1}{\vartheta^{2(m-2)}} f^{(1)}(0) \\ &- \frac{1}{\vartheta^{2(m-1)}}\big[\vartheta^2\big(e^{-t/\vartheta^2} - 1\big)\big]\big[f^{(0)}(0) + f(t)\big]. \end{aligned}$$

Substituting I into equation (1), we have

$$\begin{aligned} T[D^\alpha f(t)] = \frac{\vartheta^{2(m-\alpha)}}{\vartheta}\int_0^\infty e^{-t/\vartheta^2}\frac{1}{\vartheta}\Big[&- f^{(m-1)}(0) - \frac{1}{\vartheta^2} f^{(m-2)}(0) - \cdots \\ &- \frac{1}{\vartheta^{2(m-2)}} f^{(1)}(0) - \frac{1}{\vartheta^{2(m-1)}}\vartheta^2\big[f^{(0)}(0) - f(t)\big]\Big]\,dt. \end{aligned} \tag{35}$$

This rearranges to

$$T[D^\alpha f(t)] = \frac{\vartheta^{2(m-\alpha)-1}\,\vartheta}{\vartheta^{2(m-1)}}\int_0^\infty e^{-t/\vartheta^2} f(t)\,dt - \sum_{i=1}^{n} \vartheta^{\,2(i-\alpha)-1} f^{(i-1)}(0).$$

Thus,

$$T[D^\alpha f(t)] = \vartheta^{-2\alpha} F(\vartheta) - \sum_{i=1}^{n} \vartheta^{\,2(i-\alpha)-1} f^{(i-1)}(0),$$

that is,

$$T[D^\alpha f(t)] = \frac{1}{\vartheta^{2\alpha}}\,F(\vartheta) - \sum_{i=1}^{n} \vartheta^{\,2(i-\alpha)-1} f^{(i-1)}(0).$$

□

Exact Solution for Test Example 1. Exact solution corresponds to the classical analytical solution for $\alpha = 1$. When $\alpha = 1$, the equation (17) reduces to

$$U_t = U_{xx} + U_x, \quad U(x,0) = x.$$

We try a trial solution linear in x:

$$U(x,t) = A(t)\,x + B(t).$$

Then

$$U_x = A(t), \quad U_{xx} = 0, \quad U_t = A'(t)\,x + B'(t).$$

Substituting into the PDE gives

$$A'(t)\,x + B'(t) = A(t).$$

Equating coefficients of x and constants, we obtain

$$A'(t) = 0 \quad \Rightarrow \quad A(t) = 1 \quad (\text{from } A(0) = 1),$$

$$B'(t) = A(t) = 1 \quad \Rightarrow \quad B(t) = t \quad (\text{from } B(0) = 0).$$

Hence, the exact solution for $\alpha = 1$ is

$$U(x,t) = x + t.$$

if we put $\alpha = 1$ in the obtained solution of test example 1 using TPDTM

$$U(x,t) = x + \frac{t^{\alpha}}{\Gamma(\alpha+1)}.$$

we will get the

$$U(x,t) = x + t.$$

Similarly, we can obtain the rest of test example's exact solutions.

Received: June 2025
Accepted: August 2025

Department of Statistics and Applied Mathematics, Central University of Tamil Nadu, Neelakudi, Thiruvarur-610005, Tamil Nadu, India.
Email address: narsimhulu@cutn.ac.in

Department of Statistics and Applied Mathematics, Central University of Tamil Nadu, Neelakudi, Thiruvarur-610005, Tamil Nadu, India.
Email address: athirakinakkal2022@gmail.com